

A local adaptive discontinuous Galerkin method for convection-diffusion-reaction equations

Assyr Abdulle¹ and Giacomo Rosilho de Souza^{*1}

¹ANMC, Institute of Mathematics, École Polytechnique Fédérale de Lausanne, 1015 Lausanne, Switzerland

December 13, 2021

Abstract

We introduce a local adaptive discontinuous Galerkin method for convection-diffusion-reaction equations. The proposed method is based on a coarse grid and iteratively improves the solution's accuracy by solving local elliptic problems in refined subdomains. For purely diffusion problems, we already proved that this scheme converges under minimal regularity assumptions [A. Abdulle and G. Rosilho de Souza, *ESAIM: M2AN*, 53(4):1269–1303, 2019]. In this paper, we provide an algorithm for the automatic identification of the local elliptic problems' subdomains employing a flux reconstruction strategy. Reliable error estimators are derived for the local adaptive method. Numerical comparisons with a classical nonlocal adaptive algorithm illustrate the efficiency of the method.

Key words. elliptic equation, local scheme, discontinuous Galerkin, a posteriori error estimators
AMS subject classifications. 65N15, 65N30.

1 Introduction

Solutions to partial differential equations that exhibit singularity (e.g. cracks) or high variations in the computational domain are usually approximated by adaptive numerical methods. There is nowadays a large body of literature concerned with the development of reliable a posteriori error estimators aiming for mesh refinement in regions of large errors (see e.g. [5, 6, 7, 29]). However, classical adaptive methods are usually based on iterative processes which rely on recomputing the solution on the whole computational domain for each new mesh obtained after a refinement procedure.

In this paper we present a scheme which solves local problems defined on refined regions only. Local schemes have been proposed in the past, we mention the Local Defect Correction (LDC) method [19], the Fast Adaptive Composite (FAC) grid algorithm [23] and the Multi-Level Adaptive (MLA) technique [9]. At each iteration, these algorithms solve a problem on a coarse mesh on the whole domain and a local problem on a finer mesh. The coarse solution is used for artificial boundary conditions while the local solution is used to correct the residual in the coarse grid. In [8] the LDC scheme has been coupled with error estimators, which are used to select the local domain.

^{*}Corresponding author. E-mail address: giacomo.rosilhodesouza@epfl.ch.

In [1] we proposed a Local Discontinuous Galerkin Gradient Discretization (LDGGD) method which decomposes the computational domain in local subdomains encompassing the large gradient regions. This scheme iteratively improves a coarse solution on the full domain by solving local elliptic problems on finer meshes. Hence, the full problem is solved only in the first iteration on a coarse mesh while a sequence of solutions on smaller subdomains are subsequently computed. In turn iterations between subdomains are not needed as in the LDC, FAC or MLA schemes and the condition number of the small systems are considerably smaller than the one of large systems (which describe data and mesh variations on the whole domain). The LDGGD method has been shown to converge under minimal regularity assumptions, i.e. when the solution is in $H_0^1(\Omega)$ and the forcing term in $H^{-1}(\Omega)$ [1]. However, the marking of the subdomains this scheme did so far rely on the a priori knowledge of the location of high gradient regions.

The main contribution of this paper is to propose an adaptive local LDGGD method. This adaptive method is based on a posteriori error estimators that automatically identify the subdomains to be refined. This is crucial for practical applications of the method. The LDGGD relies on the symmetric weighted interior penalty Galerkin (SWIPG) method [13, 18] and we consider linear advection-diffusion-reaction equations

$$\begin{aligned} -\nabla \cdot (A\nabla u) + \beta \cdot \nabla u + \mu u &= f && \text{in } \Omega, \\ u &= 0 && \text{in } \partial\Omega, \end{aligned} \tag{1.1}$$

where Ω is an open bounded polytopal connected subset of \mathbb{R}^d for $d \geq 2$, A is the diffusion tensor, β the velocity field, μ the reaction coefficient and f a forcing term. In [17] the authors introduce a posteriori error estimators for the SWIPG scheme based on cutoff functions and conforming flux and potential reconstructions, these estimators are shown to be efficient and robust in singularly perturbed regimes. Following the same strategy, we derive estimators for the local scheme by weakening the regularity requirements on the reconstructed fluxes. The new estimators are as well free of unknown constants and their robustness is verified numerically. Furthermore, they are employed to define the local subdomains and provide error bounds on the numerical solution of the LDGGD method. We prove that the error estimators are reliable. Because of the local nature of our scheme, we introduce two new estimators that measure the jumps at the boundaries of the local domains. However, these two new terms have lower convergence rate than the other terms and we cannot establish the efficiency of our a posteriori estimators with our current approach. Nevertheless, the two new terms are useful in our algorithm: whenever the errors are localized these new terms become negligible; in contrast, when these estimators dominate it is an indication that the error is not localized and one can switch to a nonlocal method. Other boundary conditions than those of (1.1) can be considered, at the cost of modifying the error estimators introduced in [17]. The new estimators introduced here need no changes.

The outline of the paper is as follows. In Section 2 we describe the local scheme, in Section 3 we introduce the error estimators and state the main a posteriori error analysis results. Section 4 is dedicated to the definition of the reconstructed fluxes and proofs of the main results. Finally, various numerical examples illustrating the efficiency, versatility and limits of the proposed method are presented in Section 5.

2 Local adaptive discontinuous Galerkin method

In this section we introduce the local algorithm based on the discontinuous Galerkin method. We start by some assumptions on the data and the domain, before introducing the weak form corresponding to (1.1). We assume that $\Omega \subset \mathbb{R}^d$ is a polytopal domain with $d \geq 2$, $\beta \in W^{1,\infty}(\Omega)^d$,

$\mu \in L^\infty(\Omega)$ and $A \in L^\infty(\Omega)^{d \times d}$, with $A(\mathbf{x})$ a symmetric piecewise constant matrix with eigenvalues in $[\underline{\lambda}, \bar{\lambda}]$, where $\bar{\lambda} \geq \underline{\lambda} > 0$. Moreover, we assume that $\mu - \frac{1}{2} \nabla \cdot \boldsymbol{\beta} \geq 0$ a.e. in Ω . This term $\mu - \frac{1}{2} \nabla \cdot \boldsymbol{\beta}$ appears in the symmetric part of the operator $\mathcal{B}(\cdot, \cdot)$ defined in (2.2) and hence the assumption $\mu - \frac{1}{2} \nabla \cdot \boldsymbol{\beta} \geq 0$ is needed for coercivity. Finally, we set $f \in L^2(\Omega)$. Under these assumptions, the unique weak solution $u \in H_0^1(\Omega)$ of (1.1) satisfies

$$\mathcal{B}(u, v) = \int_{\Omega} f v \, d\mathbf{x} \quad \text{for all } v \in H_0^1(\Omega), \quad (2.1)$$

where

$$\mathcal{B}(u, v) = \int_{\Omega} (A \nabla u \cdot \nabla v + (\boldsymbol{\beta} \cdot \nabla u) v + \mu u v) \, d\mathbf{x}. \quad (2.2)$$

2.1 Preliminary definitions

We start by collecting some notations related to the geometry and the mesh of the subdomains, before recalling the definition of the discontinuous Galerkin finite element method.

Subdomains and meshes

Let $M \in \mathbb{N}$ and $\{\Omega_k\}_{k=1}^M$ be a sequence of open subdomains of Ω with $\Omega_1 = \Omega$. The domains Ω_k for $k \geq 2$ can be any polytopal subset of Ω , in practice they will be chosen by the error estimators (see Section 2.2). We consider $\{\mathcal{M}_k\}_{k=1}^M$ a sequence of simplicial meshes on Ω and $\mathcal{F}_k = \mathcal{F}_{k,b} \cup \mathcal{F}_{k,i}$ is the set of boundary and internal faces of \mathcal{M}_k . The assumption below ensures that \mathcal{M}_{k+1} is a refinement of \mathcal{M}_k inside the subdomain Ω_{k+1} .

Assumption 2.1.

1. For each $k = 1, \dots, M$, $\bar{\Omega}_k = \cup_{K \in \mathcal{M}_k, K \subset \Omega_k} \bar{K}$.
2. For $k = 1, \dots, M-1$,
 - a) $\{K \in \mathcal{M}_{k+1} : K \subset \Omega \setminus \Omega_{k+1}\} = \{K \in \mathcal{M}_k : K \subset \Omega \setminus \Omega_{k+1}\}$,
 - b) if $K, T \in \mathcal{M}_k$ with $K \subset \Omega_{k+1}$, $T \subset \Omega \setminus \Omega_{k+1}$ and $\partial K \cap \partial T \neq \emptyset$ then $K \in \mathcal{M}_{k+1}$,
 - c) if $K \in \mathcal{M}_k$ and $K \subset \Omega_{k+1}$, either $K \in \mathcal{M}_{k+1}$ or K is a union of elements in \mathcal{M}_{k+1} .

Let $\widehat{\mathcal{M}}_k = \{K \in \mathcal{M}_k : K \subset \Omega_k\}$ and $\widehat{\mathcal{F}}_k = \widehat{\mathcal{F}}_{k,b} \cup \widehat{\mathcal{F}}_{k,i}$ the set of faces of $\widehat{\mathcal{M}}_k$, with $\widehat{\mathcal{F}}_{k,b}$ and $\widehat{\mathcal{F}}_{k,i}$ the boundary and internal faces, respectively. Condition 1 in Assumption 2.1 ensures that $\widehat{\mathcal{M}}_k$ is a simplicial mesh on Ω_k . Condition 2 guarantees that in $\Omega \setminus \Omega_{k+1}$ and in the neighborhood of $\partial \Omega_{k+1} \setminus \partial \Omega$ the meshes \mathcal{M}_k and \mathcal{M}_{k+1} are equal and that \mathcal{M}_{k+1} is a refinement of \mathcal{M}_k in Ω_{k+1} . An example of domains and meshes satisfying Assumption 2.1 is illustrated in Figure 1.

Discontinuous Galerkin finite element method

The local adaptive discontinuous Galerkin method will solve local elliptic problems in Ω_k by using a discontinuous Galerkin scheme introduced in [18], which we recall here. In what follows, $\mathfrak{T} = (D, \mathcal{M}, \mathcal{F})$ denotes a tuple defined by a domain D , a simplicial mesh \mathcal{M} on D and its set of faces $\mathcal{F} = \mathcal{F}_b \cup \mathcal{F}_i$. In practice we will consider $\mathfrak{T}_k = (\Omega, \mathcal{M}_k, \mathcal{F}_k)$ or $\widehat{\mathfrak{T}}_k = (\Omega_k, \widehat{\mathcal{M}}_k, \widehat{\mathcal{F}}_k)$. For $\mathfrak{T} = (D, \mathcal{M}, \mathcal{F})$ we define

$$V(\mathfrak{T}) = \{v \in L^2(D) : v|_K \in \mathbb{P}_\ell(K), \forall K \in \mathcal{M}\}, \quad (2.3)$$

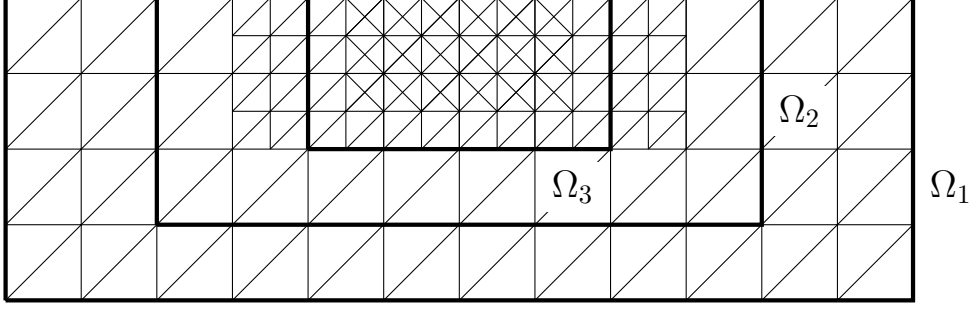


Figure 1. Example of possible meshes for three embedded domains Ω_1 , Ω_2 , Ω_3 .

where $\mathbb{P}_\ell(K)$ is the set of polynomials in K of total degree ℓ . As usual for such discontinuous Galerkin methods we need to define appropriate averages, jumps, weights and penalization parameters. For $K \in \mathcal{M}$ we denote \mathbf{n}_K the unit normal outward to K and $\mathcal{F}_K = \{\sigma \in \mathcal{F} : \sigma \subset \partial K\}$. Let $\sigma \in \mathcal{F}_i$ and $K, T \in \mathcal{M}$ with $\sigma = \partial K \cap \partial T$, then $\mathbf{n}_\sigma = \mathbf{n}_K$ and

$$\delta_{K,\sigma} = \mathbf{n}_\sigma^\top A|_K \mathbf{n}_\sigma, \quad \delta_{T,\sigma} = \mathbf{n}_\sigma^\top A|_T \mathbf{n}_\sigma.$$

The weights are defined by

$$\omega_{K,\sigma} = \frac{\delta_{T,\sigma}}{\delta_{K,\sigma} + \delta_{T,\sigma}}, \quad \omega_{T,\sigma} = \frac{\delta_{K,\sigma}}{\delta_{K,\sigma} + \delta_{T,\sigma}}$$

and the penalization parameters by

$$\gamma_\sigma = 2 \frac{\delta_{K,\sigma} \delta_{T,\sigma}}{\delta_{K,\sigma} + \delta_{T,\sigma}}, \quad \nu_\sigma = \frac{1}{2} |\boldsymbol{\beta} \cdot \mathbf{n}_\sigma|.$$

If $\sigma \in \mathcal{F}_b$ and $K \in \mathcal{M}$ with $\sigma = \partial K \cap \partial D$ then \mathbf{n}_σ is \mathbf{n}_D the unit outward normal to ∂D and

$$\delta_{K,\sigma} = \mathbf{n}_\sigma^\top A|_K \mathbf{n}_\sigma, \quad \omega_{K,\sigma} = 1, \quad \gamma_\sigma = \delta_{K,\sigma}, \quad \nu_\sigma = \frac{1}{2} |\boldsymbol{\beta} \cdot \mathbf{n}_\sigma|.$$

Let $g \in L^2(\partial D)$, we define the averages and jumps of $v \in V(\mathfrak{T})$ as follows. For $\sigma \in \mathcal{F}_b$ with $\sigma = \partial K \cap \partial D$ we set

$$\{\!\!\{v\}\!\!\}_\omega, \sigma = v|_K, \quad \{\!\!\{v\}\!\!\}_g, \sigma = \frac{1}{2}(v|_K + g), \quad \llbracket v \rrbracket_{g,\sigma} = v|_K - g$$

and for $\sigma \in \mathcal{F}_i$ with $\sigma = \partial K \cap \partial T$

$$\{\!\!\{v\}\!\!\}_\omega, \sigma = \omega_{K,\sigma} v|_K + \omega_{T,\sigma} v|_T, \quad \{\!\!\{v\}\!\!\}_g, \sigma = \frac{1}{2}(v|_K + v|_T), \quad \llbracket v \rrbracket_{g,\sigma} = v|_K - v|_T.$$

We define $\llbracket \cdot \rrbracket_\sigma = \llbracket \cdot \rrbracket_{0,\sigma}$ and $\{\!\!\{ \cdot \}\!\!\}_\sigma = \{\!\!\{ \cdot \}\!\!\}_{0,\sigma}$. A similar notation holds for vector valued functions and whenever no confusion can arise the subscript σ is omitted. Let h_σ be the diameter of σ and $\eta_\sigma > 0$

a user parameter, for $u, v \in V(\mathfrak{T})$ we define the bilinear form

$$\begin{aligned}
\mathcal{B}(u, v, \mathfrak{T}, g) &= \int_D (A \nabla u \cdot \nabla v + (\mu - \nabla \cdot \boldsymbol{\beta}) u v - u \boldsymbol{\beta} \cdot \nabla v) \, d\mathbf{x} \\
&\quad - \sum_{\sigma \in \mathcal{F}} \int_{\sigma} (\llbracket v \rrbracket \{ \{ A \nabla u \} \}_{\omega} \cdot \mathbf{n}_{\sigma} + \llbracket u \rrbracket_g \{ \{ A \nabla v \} \}_{\omega} \cdot \mathbf{n}_{\sigma}) \, d\mathbf{y} \\
&\quad + \sum_{\sigma \in \mathcal{F}} \int_{\sigma} ((\eta_{\sigma} \frac{\gamma_{\sigma}}{h_{\sigma}} + \nu_{\sigma}) \llbracket u \rrbracket_g \llbracket v \rrbracket + \boldsymbol{\beta} \cdot \mathbf{n}_{\sigma} \{ \{ u \} \}_g \llbracket v \rrbracket) \, d\mathbf{y},
\end{aligned} \tag{2.4}$$

where the gradients are taken element wise. The bilinear form $\mathcal{B}(\cdot, \cdot, \mathfrak{T}, g)$ will be used to approximate elliptic problems in D with Dirichlet boundary condition g . This scheme is known as the Symmetric Weighted Interior Penalty (SWIP) scheme [18]. The SWIP method is an improvement of the Interior Penalty scheme (IP) [4], where the weights are defined as $\omega_{K,\sigma} = \omega_{T,\sigma} = 1/2$. The use of diffusivity-dependent averages increases the robustness of the method for problems with strong diffusion discontinuities. The bilinear form defined in (2.4) is mathematically equivalent to other formulations where $v \boldsymbol{\beta} \cdot \nabla u$ or $\nabla \cdot (\boldsymbol{\beta} u) v$ appear instead of $u \boldsymbol{\beta} \cdot \nabla v$ (see [18] and [13, Section 4.6.2]). Our choice of formulation is convenient to express local conservation laws (see [13, Section 2.2.3]).

2.2 Local method algorithm

In this section we present the local scheme. In order to facilitate the comprehension of the method, we start with an informal description and then provide a pseudo-code for the algorithm. We denote u_k the global solutions on Ω and \hat{u}_k the local solutions on Ω_k , which are used to correct the global solutions.

Given a discretization $\mathfrak{T}_1 = (\Omega, \mathcal{M}_1, \mathcal{F}_1)$ on Ω the local scheme computes a first approximate solution $u_1 \in V(\mathfrak{T}_1)$ to (2.1). The algorithm then performs the following steps for $k = 2, \dots, M$.

- i) Given the current solution u_{k-1} , identify the region Ω_k where the error is large and define a new refined mesh \mathcal{M}_k satisfying Assumption 2.1 by iterating the following steps.
 - a) For each element $K \in \mathcal{M}_{k-1}$ compute an error indicator $\eta_{M,K}$ (defined in (3.5)) and mark the local domain Ω_k using the fixed energy fraction marking strategy [14, Section 4.2]. Hence, Ω_k is defined as the union of the elements with largest error indicator $\eta_{M,K}$ and it is such that the error committed inside of Ω_k is at least a prescribed fraction of the total error.
 - b) Define the new mesh \mathcal{M}_k by refining the elements $K \in \mathcal{M}_{k-1}$ with $K \subset \Omega_k$.
 - c) Enlarge the local domain Ω_k defined at step a) by adding a one element wide boundary layer (i.e. in order to satisfy item 2b of Assumption 2.1).
 - d) Define the local mesh $\widehat{\mathcal{M}}_k$ by the elements of \mathcal{M}_k inside of Ω_k .
- ii) Solve a local elliptic problem in Ω_k on the refined mesh $\widehat{\mathcal{M}}_k$ using u_{k-1} as artificial Dirichlet boundary condition on $\partial\Omega_k \setminus \partial\Omega$. The solution is denoted $\hat{u}_k \in V(\widehat{\mathfrak{T}}_k)$, where $\widehat{\mathfrak{T}}_k = (\Omega_k, \widehat{\mathcal{M}}_k, \widehat{\mathcal{F}}_k)$.
- iii) The local solution \hat{u}_k is used to correct the previous solution u_{k-1} inside of Ω_k and obtain the new global solution u_k .

The pseudo-code of the local scheme is given in Algorithm 1, where $\chi_{\Omega \setminus \Omega_k}$ is the indicator function of $\Omega \setminus \Omega_k$ and $(\cdot, \cdot)_k$ is the inner product in $L^2(\Omega_k)$. The function $\text{LocalDomain}(u_k, \mathfrak{T}_k)$ used in Algorithm 1 performs steps a)-d) of i). For purely diffusive problems, it is shown in [27, Theorem 8.2] that Algorithm 1 is equivalent to the LDGGD introduced in [1], hence the scheme converges for exact solutions $u \in H_0^1(\Omega)$.

Algorithm 1 LocalScheme(\mathfrak{T}_1)

Find $u_1 \in V(\mathfrak{T}_1)$ solution to $\mathcal{B}(u_1, v_1, \mathfrak{T}_1, 0) = (f, v_1)_1$ for all $v_1 \in V(\mathfrak{T}_1)$.
for $k = 2, \dots, M$ **do**
 $(\mathfrak{T}_k, \widehat{\mathfrak{T}}_k) = \text{LocalDomain}(u_{k-1}, \mathfrak{T}_{k-1})$.
 $g_k = u_{k-1} \chi_{\Omega \setminus \Omega_k} \in V(\mathfrak{T}_k)$.
 Find $\hat{u}_k \in V(\widehat{\mathfrak{T}}_k)$ solution to $\mathcal{B}(\hat{u}_k, v_k, \widehat{\mathfrak{T}}_k, g_k) = (f, v_k)_k$ for all $v_k \in V(\widehat{\mathfrak{T}}_k)$.
 $u_k = g_k + \hat{u}_k \in V(\mathfrak{T}_k)$.
end for

3 Error estimators via flux and potential reconstructions

The error estimators used to mark the local domains Ω_k and to provide error bounds on the numerical solution u_k are introduced here.

In the framework of selfadjoint elliptic problems, the equilibrated fluxes method [3, 7] is a technique largely used to derive a posteriori error estimators free of undetermined constants and is based on the definition of local fluxes which satisfy a local conservation property. Since local fluxes and conservation properties are intrinsic to the discontinuous Galerkin formulation, this discretization is well suited for the equilibrated fluxes method [2, 12]. In [15, 21] the Raviart-Thomas-Nédélec space is used to build an $H_{\text{div}}(\Omega)$ conforming reconstruction \mathbf{t}_h of the discrete diffusive flux $-A\nabla u_h$. A diffusive flux \mathbf{t}_h with optimal divergence, in the sense that it coincides with the orthogonal projection of the right-hand side f onto the discontinuous Galerkin space, is obtained. In [17] the authors extend this approach to convection-diffusion-reaction equations by defining an $H_{\text{div}}(\Omega)$ conforming convective flux \mathbf{q}_h approximating βu_h and satisfying a conservation property.

We follow a similar strategy and define in the next section error estimators in function of diffusive and convective fluxes reconstructions $\mathbf{t}_k, \mathbf{q}_k$ for the local scheme, as well as an $H_0^1(\Omega)$ conforming potential reconstruction s_k of the solution u_k .

3.1 Definition of the error estimators

The error estimators in function of the potential reconstruction s_k approximating the solution u_k , the diffusive and convective fluxes \mathbf{t}_k and \mathbf{q}_k approximating $-A\nabla u_k$ and βu_k , respectively, are defined in this section.

Following the iterative and local nature of our scheme, we define the diffusive and convective fluxes reconstructions as

$$\mathbf{t}_k = \mathbf{t}_{k-1} \chi_{\Omega \setminus \Omega_k} + \hat{\mathbf{t}}_k, \quad \mathbf{q}_k = \mathbf{q}_{k-1} \chi_{\Omega \setminus \Omega_k} + \hat{\mathbf{q}}_k, \quad (3.1)$$

where $\mathbf{t}_0 = \mathbf{q}_0 = 0$ and $\hat{\mathbf{t}}_k, \hat{\mathbf{q}}_k$ are $H_{\text{div}}(\Omega_k)$ conforming fluxes reconstructions of $-A\nabla \hat{u}_k, \beta \hat{u}_k$, respectively, and where \hat{u}_k is the local solution. To avoid any abuse of notation in (3.1), we extended $\hat{\mathbf{t}}_k, \hat{\mathbf{q}}_k$ to zero outside of Ω_k . The fluxes reconstructions $\hat{\mathbf{t}}_k, \hat{\mathbf{q}}_k$ satisfy a local conservation property

and are defined in Section 4.1. We readily see that (3.1) allows for flux jumps at the subdomains boundaries, while giving enough freedom to define $\hat{\mathbf{t}}_k, \hat{\mathbf{q}}_k$ in a way that a conservation property is satisfied. The fluxes reconstructions are used to measure the non conformity of the numerical fluxes. In the same spirit we define a potential reconstruction $s_k \in H_0^1(\Omega)$ used to measure the non conformity of the numerical solution. It is defined recursively as

$$s_k = s_{k-1}\chi_{\Omega \setminus \Omega_k} + \hat{s}_k, \quad (3.2)$$

where $s_0 = 0$ and $\hat{s}_k \in H^1(\Omega_k)$ is such that $s_k \in H_0^1(\Omega)$; similarly, we extend \hat{s}_k to zero outside of Ω_k . More details about the definitions of $\hat{\mathbf{t}}_k, \hat{\mathbf{q}}_k$ and \hat{s}_k will be given in Section 4.1, for the time being we will define the error estimators.

Let $K \in \mathcal{M}_k, v \in H^1(K)$,

$$\|v\|_K^2 = \|A^{1/2}\nabla v\|_{L^2(K)^d}^2 + \|(\mu - \frac{1}{2}\nabla \cdot \boldsymbol{\beta})^{1/2}v\|_{L^2(K)}^2, \quad (3.3)$$

where $\|\cdot\|_{L^2(K)}$ is the L^2 -norm for scalar-valued functions in K and $\|\cdot\|_{L^2(K)^d}$ the L^2 -norm for vector-valued functions in K . The non conformity of the numerical solution u_k is measured by the estimator

$$\eta_{NC,K} = \|u_k - s_k\|_K. \quad (3.4a)$$

In the following, $m_K, \tilde{m}_K, m_\sigma, D_{t,K,\sigma}, c_{\boldsymbol{\beta},\mu,K} > 0$ are some known constants which will be defined in Section 4.2. The residual estimator is

$$\eta_{R,K} = m_K \|f - \nabla \cdot \mathbf{t}_k - \nabla \cdot \mathbf{q}_k - (\mu - \nabla \cdot \boldsymbol{\beta})u_k\|_{L^2(K)}, \quad (3.4b)$$

which can be seen as the residual of (2.1) where we first replace u by u_k , then $-A\nabla u_k$ by $\mathbf{t}_k, \boldsymbol{\beta}u_k$ by \mathbf{q}_k and finally use the Green theorem. The error estimators defined in (3.4c) to (3.4j) measure the error introduced by these substitutions and the error introduced when applying the Green theorem to $\mathbf{t}_k, \mathbf{q}_k$, which are not in $H_{\text{div}}(\Omega)$.

The diffusive flux estimator measures the difference between $-A\nabla u_k$ and \mathbf{t}_k . It is given by $\eta_{DF,K} = \min\{\eta_{DF,K}^1, \eta_{DF,K}^2\}$, where

$$\begin{aligned} \eta_{DF,K}^1 &= \|A^{1/2}\nabla u_k + A^{-1/2}\mathbf{t}_k\|_{L^2(K)^d}, \\ \eta_{DF,K}^2 &= m_K \|(\mathcal{I} - \pi_0)(\nabla \cdot (A\nabla u_k + \mathbf{t}_k))\|_{L^2(K)} \\ &\quad + \tilde{m}_K^{1/2} \sum_{\sigma \in \mathcal{F}_K} C_{t,K,\sigma}^{1/2} \|(A\nabla u_k + \mathbf{t}_k) \cdot \mathbf{n}_\sigma\|_{L^2(\sigma)}, \end{aligned} \quad (3.4c)$$

π_0 is the L^2 -orthogonal projector onto $\mathbb{P}_0(K)$ and \mathcal{I} is the identity operator. Let $\sigma \in \mathcal{F}_k$ and $\pi_{0,\sigma}$ be the L^2 -orthogonal projector onto $\mathbb{P}_0(\sigma)$. The convection and upwinding estimators, that measure the difference between $\boldsymbol{\beta}u_k, \boldsymbol{\beta}s_k$ and \mathbf{q}_k , are defined by

$$\eta_{C,1,K} = m_K \|(\mathcal{I} - \pi_0)(\nabla \cdot (\mathbf{q}_k - \boldsymbol{\beta}s_k))\|_{L^2(K)}, \quad (3.4d)$$

$$\eta_{C,2,K} = \frac{1}{2}c_{\boldsymbol{\beta},\mu,K}^{-1/2} \|(\nabla \cdot \boldsymbol{\beta})(u_k - s_k)\|_{L^2(K)}, \quad (3.4e)$$

$$\tilde{\eta}_{C,1,K} = \tilde{m}_K \|(\mathcal{I} - \pi_0)(\nabla \cdot (\mathbf{q}_k - \boldsymbol{\beta}u_k))\|_{L^2(K)}, \quad (3.4f)$$

$$\eta_{U,K} = \sum_{\sigma \in \mathcal{F}_K} \chi_\sigma m_\sigma \|\pi_{0,\sigma}\{\{\mathbf{q}_k - \boldsymbol{\beta}s_k\}\} \cdot \mathbf{n}_\sigma\|_{L^2(\sigma)}, \quad (3.4g)$$

$$\tilde{\eta}_{U,K} = \sum_{\sigma \in \mathcal{F}_K} \chi_\sigma m_\sigma \|\pi_{0,\sigma}\{\{\mathbf{q}_k - \boldsymbol{\beta}u_k\}\} \cdot \mathbf{n}_\sigma\|_{L^2(\sigma)}, \quad (3.4h)$$

where $\chi_\sigma = 2$ if $\sigma \in \mathcal{F}_{k,b}$ and $\chi_\sigma = 1$ if $\sigma \in \mathcal{F}_{k,i}$. Finally, we introduce the jump estimators coming from the application of the Green theorem to \mathbf{t}_k and \mathbf{q}_k (see Lemma 4.4). Those are defined by

$$\eta_{\Gamma,1,K} = \frac{1}{2}(|K|c_{\beta,\mu,K})^{-1/2} \sum_{\sigma \in \overline{\mathcal{F}_K} \cap \mathcal{F}_{k,i}} \|\pi_{0,\sigma} \llbracket \mathbf{q}_k \rrbracket \cdot \mathbf{n}_\sigma\|_{L^1(\sigma)}, \quad (3.4i)$$

$$\eta_{\Gamma,2,K} = \frac{1}{2} \sum_{\sigma \in \mathcal{F}_K \cap \mathcal{F}_{k,i}} D_{t,K,\sigma} \|\llbracket \mathbf{t}_k \rrbracket \cdot \mathbf{n}_\sigma\|_{L^2(\sigma)}. \quad (3.4j)$$

We end the section defining the marking error estimator $\eta_{M,K}$ used to mark Ω_k in the LocalDomain routine of Algorithm 1, let

$$\begin{aligned} \eta_{M,K} = & \eta_{NC,K} + \eta_{R,K} + \eta_{DF,K} + \eta_{C,1,K} + \eta_{C,2,K} + \eta_{U,K} \\ & + \eta_{\Gamma,1,K} + \eta_{\Gamma,2,K} + \tilde{\eta}_{C,1,K} + \tilde{\eta}_{U,K}. \end{aligned} \quad (3.5)$$

3.2 Main results

We state here our main results related to the a posteriori analysis of the local scheme, in particular we will provide reliable error bounds on the numerical solution u_k which are free of undetermined constants. We will also comment as to why we cannot prove the efficiency of the new estimator.

We start defining the norms for which we provide the error bounds, the same norms are used in [17]. The operator \mathcal{B} defined in (2.2) can be written $\mathcal{B} = \mathcal{B}_S + \mathcal{B}_A$, where \mathcal{B}_S and \mathcal{B}_A are symmetric and skew-symmetric operators defined by

$$\begin{aligned} \mathcal{B}_S(u, v) &= \int_{\Omega} (A \nabla u \cdot \nabla v + (\mu - \frac{1}{2} \nabla \cdot \boldsymbol{\beta}) uv) \, d\mathbf{x}, \\ \mathcal{B}_A(u, v) &= \int_{\Omega} (\boldsymbol{\beta} \cdot \nabla u + \frac{1}{2} (\nabla \cdot \boldsymbol{\beta}) u) v \, d\mathbf{x}, \end{aligned}$$

for $u, v \in H^1(\mathcal{M}_k)$. The energy norm is defined by the symmetric operator as

$$\|v\|^2 = \mathcal{B}_S(v, v) = \|A^{1/2} \nabla v\|_{L^2(\Omega)^d}^2 + \|(\mu - \frac{1}{2} \nabla \cdot \boldsymbol{\beta})^{1/2} v\|_{L^2(\Omega)}^2,$$

observe that $\|v\|^2 = \sum_{K \in \mathcal{M}_k} \|v\|_K^2$, with $\|\cdot\|_K$ as in (3.3). Since the norm $\|\cdot\|$ is defined by the symmetric operator, it is well suited to study problems with dominant diffusion or reaction. On the other hand, it is inappropriate for convection dominated problems since it lacks a term measuring the error along the velocity direction. For this kind of problems we use the augmented norm

$$\|v\|_{\oplus} = \|v\| + \sup_{\substack{w \in H_0^1(\Omega) \\ \|w\|=1}} (\mathcal{B}_A(v, w) + \mathcal{B}_J(v, w)),$$

where

$$\mathcal{B}_J(v, w) = - \sum_{\sigma \in \mathcal{F}_{k,i}} \int_{\sigma} \llbracket \boldsymbol{\beta} v \rrbracket \cdot \mathbf{n}_\sigma \{ \pi_0 w \} \, d\mathbf{y}$$

is a term needed to sharpen the error bounds. The next two theorems give a bound on the error of the local scheme, measured in the energy or the augmented norm.

Theorem 3.1. *Let $u \in H_0^1(\Omega)$ be the solution to (2.1), $u_k \in V(\mathfrak{T}_k)$ given by Algorithm 1, $s_k \in V(\mathfrak{T}_k) \cap H_0^1(\Omega)$ from (3.2) and (4.5) and $\mathbf{t}_k, \mathbf{q}_k \in \mathbf{RTN}_z(\mathcal{M}_k)$ be defined by (3.1) and (4.2). Then, the error measured in the energy norm is bounded as*

$$\|u - u_k\| \leq \eta = \left(\sum_{K \in \mathcal{M}_k} \eta_{NC,K}^2 \right)^{1/2} + \left(\sum_{K \in \mathcal{M}_k} \eta_{1,K}^2 \right)^{1/2},$$

where $\eta_{1,K} = \eta_{R,K} + \eta_{DF,K} + \eta_{C,1,K} + \eta_{C,2,K} + \eta_{U,K} + \eta_{\Gamma,1,K} + \eta_{\Gamma,2,K}$.

Theorem 3.2. *Under the same assumptions of Theorem 3.1, the error measured in the augmented norm is bounded as*

$$\|u - u_k\|_{\oplus} \leq \tilde{\eta} = 2\eta + \left(\sum_{K \in \mathcal{M}_k} \eta_{2,K}^2 \right)^{1/2},$$

with η from Theorem 3.1 and $\eta_{2,K} = \eta_{R,K} + \eta_{DF,K} + \tilde{\eta}_{C,1,K} + \tilde{\eta}_{U,K} + \eta_{\Gamma,1,K} + \eta_{\Gamma,2,K}$.

The error estimators of Theorems 3.1 and 3.2 are free of undetermined constants, indeed they depend on the numerical solution, the smallest eigenvalues of the diffusion tensor, on the essential minimum of $\mu - \frac{1}{2}\nabla \cdot \boldsymbol{\beta}$, the mesh size and known geometric constants. In contrast, the error estimators are not efficient. The reason is that, compared to the true errors $\|u - u_k\|$ and $\|u - u_k\|_{\oplus}$, the error estimators $\eta_{\Gamma,1,K}, \eta_{\Gamma,2,K}$ have a lower order of convergence. We illustrate this numerically in Section 5.1. However, $\eta_{\Gamma,1,K}, \eta_{\Gamma,2,K}$ are useful in practice: whenever they are small, then the error estimators are efficient. When they become large then they indicate that the error is not localized and one should switch to a nonlocal method. This is also illustrated numerically in Section 5.1.

4 Potential and fluxes reconstructions, proofs of the main results

In this section, we will define the potential, diffusion and advection reconstructions, define the geometric constants appearing in the error estimators defined in (3.4a) to (3.4j) and finally prove Theorems 3.1 and 3.2.

4.1 Potential and fluxes reconstruction via the equilibrated flux method

We define here the fluxes reconstructions $\hat{\mathbf{t}}_k, \hat{\mathbf{q}}_k$ of (3.1) and the potential reconstruction \hat{s}_k of (3.2). In what follows we assume that \mathcal{M}_k does not have hanging nodes, i.e. we consider matching meshes, since it simplifies the analysis; however, in practice nonmatching meshes possessing hanging nodes can be employed (as in Section 5). Roughly speaking, the next results are extended to nonmatching meshes by building matching submeshes and computing the error estimators on those submeshes, we refer to [17, Appendix] for the details.

We start defining some broken Sobolev spaces and then the potential and fluxes reconstructions. For $k = 1, \dots, M$ let $\mathcal{G}_k = \{G_j \mid j = 1, \dots, k\}$, where $G_k = \Omega_k$ and

$$G_j = \Omega_j \setminus \cup_{i=j+1}^k \bar{\Omega}_i \quad \text{for } j = 1, \dots, k-1.$$

In Figures 2(a) and 2(b) we give an example of a sequence of domains Ω_k and the corresponding set \mathcal{G}_k . We define the broken spaces

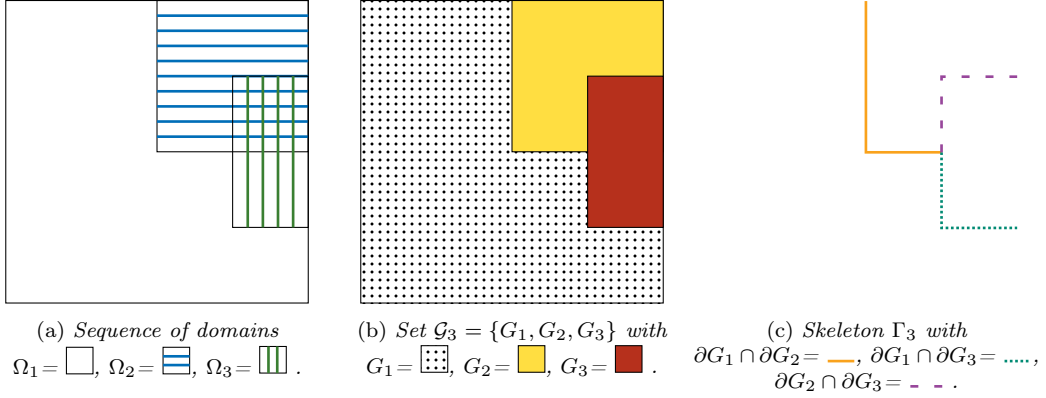


Figure 2. Example of sequence of domains $\Omega_1, \Omega_2, \Omega_3$, set \mathcal{G}_3 and skeleton Γ_3 .

$$H_{\text{div}}(\mathcal{G}_k) = \{v \in L^2(\Omega)^d : v|_G \in H_{\text{div}}(G) \text{ for all } G \in \mathcal{G}_k\},$$

$$H^1(\mathcal{M}_k) = \{v \in L^2(\Omega) : v|_K \in H^1(K) \text{ for all } K \in \mathcal{M}_k\},$$

the divergence and gradient operators in $H_{\text{div}}(\mathcal{G}_k)$ and $H^1(\mathcal{M}_k)$ are taken element wise. We extend the jump operator $[[\cdot]]_\sigma$ to the broken space $H^1(\mathcal{M}_k)$. We call Γ_k the internal skeleton of \mathcal{G}_k , that is

$$\Gamma_k = \{\partial G_i \cap \partial G_j \mid G_i, G_j \in \mathcal{G}_k, i \neq j\},$$

an example of Γ_k is given in Figure 2(c). For each $\gamma \in \Gamma_k$ we define $\mathcal{F}_\gamma = \{\sigma \in \mathcal{F}_{k,i} \mid \sigma \subset \gamma\}$ and set \mathbf{n}_γ , the normal to γ , as $\mathbf{n}_\gamma|_\sigma = \mathbf{n}_\sigma$. The jump $[[\cdot]]_\gamma$ on γ is defined by $[[\cdot]]_\gamma|_\sigma = [[\cdot]]_\sigma$.

In [17] the reconstructed fluxes live in $H_{\text{div}}(\Omega)$. For the local algorithm we need to build such fluxes using the recursive relation (3.1). This leads to fluxes having jumps across the boundaries of the subdomains, i.e. $\gamma \in \Gamma_k$, hence they lie in the broken space $H_{\text{div}}(\mathcal{G}_k)$. In the rest of this section we explain how to build fluxes which are in an approximation space of $H_{\text{div}}(\mathcal{G}_k)$ and satisfy a local conservation property. We start by introducing a broken version of the usual Raviart-Thomas-Nédélec spaces [24, 26], which we define as

$$\mathbf{RTN}_\varkappa(\mathcal{M}_k) := \{v_k \in H_{\text{div}}(\mathcal{G}_k) : v_k|_K \in \mathbf{RTN}_\varkappa(K) \text{ for all } K \in \mathcal{M}_k\}, \quad (4.1)$$

where $\varkappa \in \{\ell - 1, \ell\}$ and $\mathbf{RTN}_\varkappa(K) = \mathbb{P}_\varkappa(K)^d + \mathbf{x}\mathbb{P}_\varkappa(K)$. In order to build functions in $\mathbf{RTN}_\varkappa(\mathcal{M}_k)$ we need a characterization of this space. Let $v_k \in L^2(\Omega)^d$ such that $v_k|_K \in \mathbf{RTN}_\varkappa(K)$ for each $K \in \mathcal{M}_k$, it is known that $v_k \in H_{\text{div}}(\Omega)$ if and only if $[[v_k]]_\sigma \cdot \mathbf{n}_\sigma = 0$ for all $\sigma \in \mathcal{F}_{k,i}$ (see [13, Lemma 1.24]). Since we search for fluxes $v_k \in H_{\text{div}}(\mathcal{G}_k)$, we relax this condition and allow $[[v_k]]_\gamma \cdot \mathbf{n}_\gamma \neq 0$ for $\gamma \in \Gamma_k$.

Lemma 4.1. *Let $v_k \in L^2(\Omega)^d$ be such that $v_k|_K \in \mathbf{RTN}_\varkappa(K)$ for each $K \in \mathcal{M}_k$, then $v_k \in \mathbf{RTN}_\varkappa(\mathcal{M}_k)$ if and only if $[[v_k]]_\sigma \cdot \mathbf{n}_\sigma = 0$ for all $\sigma \notin \cup_{\gamma \in \Gamma_k} \mathcal{F}_\gamma$.*

Proof. Following the lines of [13, Lemma 1.24]. \square

The diffusive and convective fluxes $\mathbf{t}_k, \mathbf{q}_k \in \mathbf{RTN}_\varkappa(\mathcal{M}_k)$ are defined recursively as in (3.1), where $\hat{\mathbf{t}}_k, \hat{\mathbf{q}}_k \in \mathbf{RTN}_\varkappa(\widehat{\mathcal{M}}_k)$, with

$$\mathbf{RTN}_\varkappa(\widehat{\mathcal{M}}_k) := \{v_k \in H_{\text{div}}(\Omega_k) : v_k|_K \in \mathbf{RTN}_\varkappa(K) \text{ for all } K \in \widehat{\mathcal{M}}_k\},$$

are given by the relations

$$\begin{aligned}\int_{\sigma} \hat{\mathbf{t}}_k \cdot \mathbf{n}_{\sigma} p_k \, d\mathbf{y} &= \int_{\sigma} (-\{A\nabla \hat{u}_k\}_{\omega} \cdot \mathbf{n}_{\sigma} + \eta_{\sigma} \frac{\gamma_{\sigma}}{h_{\sigma}} [\hat{u}_k]_{g_k}) p_k \, d\mathbf{y}, \\ \int_{\sigma} \hat{\mathbf{q}}_k \cdot \mathbf{n}_{\sigma} p_k \, d\mathbf{y} &= \int_{\sigma} (\boldsymbol{\beta} \cdot \mathbf{n}_{\sigma} \{\hat{u}_k\}_{g_k} + \nu_{\sigma} [\hat{u}_k]_{g_k}) p_k \, d\mathbf{y}\end{aligned}\tag{4.2a}$$

for all $\sigma \in \widehat{\mathcal{F}}_k$ and $p_k \in \mathbb{P}_{\sharp}(\sigma)$ and

$$\begin{aligned}\int_K \hat{\mathbf{t}}_k \cdot \hat{\mathbf{r}}_k \, d\mathbf{x} &= - \int_K A\nabla \hat{u}_k \cdot \hat{\mathbf{r}}_k \, d\mathbf{x} + \sum_{\sigma \in \mathcal{F}_K} \int_{\sigma} \omega_{K,\sigma} [\hat{u}_k]_{g_k} A|_K \hat{\mathbf{r}}_k \cdot \mathbf{n}_{\sigma} \, d\mathbf{y}, \\ \int_K \hat{\mathbf{q}}_k \cdot \hat{\mathbf{r}}_k \, d\mathbf{x} &= \int_K \hat{u}_k \boldsymbol{\beta} \cdot \hat{\mathbf{r}}_k \, d\mathbf{x}\end{aligned}\tag{4.2b}$$

for all $K \in \widehat{\mathcal{M}}_k$ and $\hat{\mathbf{r}}_k \in \mathbb{P}_{\sharp-1}(K)^d$. Since $\hat{\mathbf{t}}_k|_K \cdot \mathbf{n}_{\sigma}, \hat{\mathbf{q}}_k|_K \cdot \mathbf{n}_{\sigma} \in \mathbb{P}_{\sharp}(\sigma)$ (see [10, Proposition 3.2]) then (4.2a) defines $\hat{\mathbf{t}}_k|_K \cdot \mathbf{n}_{\sigma}, \hat{\mathbf{q}}_k|_K \cdot \mathbf{n}_{\sigma}$ on σ . The remaining degrees of freedom are fixed by (4.2b) [10, Proposition 3.3]. Thanks to (4.2a) we have $[\hat{\mathbf{t}}_k] \cdot \mathbf{n}_{\sigma} = 0$ and $[\hat{\mathbf{q}}_k] \cdot \mathbf{n}_{\sigma} = 0$ for $\sigma \in \widehat{\mathcal{F}}_{k,i}$ and hence $\hat{\mathbf{t}}_k, \hat{\mathbf{q}}_k \in \mathbf{RTN}_{\sharp}(\widehat{\mathcal{M}}_k)$. By construction it follows $\mathbf{t}_k, \mathbf{q}_k \in \mathbf{RTN}_{\sharp}(\mathcal{M}_k)$.

Let $K \in \mathcal{M}_k$ and π_{\sharp} be the L^2 -orthogonal projector onto $\mathbb{P}_{\sharp}(K)$, the following lemma states a local conservation property of the reconstructed fluxes. The proof follows the lines of [17, Lemma 2.1]

Lemma 4.2. *Let $u_k \in V(\mathfrak{T}_k)$ be given by Algorithm 1 and $\mathbf{t}_k, \mathbf{q}_k \in H_{\text{div}}(\mathcal{G}_k)$ defined by (3.1) and (4.2). For all $K \in \mathcal{M}_k$ it holds*

$$(\nabla \cdot \mathbf{t}_k + \nabla \cdot \mathbf{q}_k + \pi_{\sharp}((\mu - \nabla \cdot \boldsymbol{\beta})u_k))|_K = \pi_{\sharp} f|_K.$$

Proof. Let $K \in \mathcal{M}_k$ and $j = \max\{i = 1, \dots, k : K \subset \Omega_j\}$, then $K \in \widehat{\mathcal{M}}_j$, $\mathbf{t}_k|_K = \hat{\mathbf{t}}_j|_K$, $\mathbf{q}_k|_K = \hat{\mathbf{q}}_j|_K$ and $u_k|_K = \hat{u}_j|_K$. Let $v_j \in \mathbb{P}_{\sharp}(K)$, with $v_j = 0$ outside of K , by the Green theorem we have

$$\int_K (\nabla \cdot \hat{\mathbf{t}}_j + \nabla \cdot \hat{\mathbf{q}}_j) v_j \, d\mathbf{x} = - \int_K (\hat{\mathbf{t}}_j + \hat{\mathbf{q}}_j) \cdot \nabla v_j \, d\mathbf{x} + \sum_{\sigma \in \mathcal{F}_K} \int_{\sigma} v_j (\hat{\mathbf{t}}_j + \hat{\mathbf{q}}_j) \cdot \mathbf{n}_K \, d\mathbf{y}\tag{4.3}$$

and using $\mathcal{B}(\hat{u}_j, v_j, \widehat{\mathfrak{T}}_j, g_j) = (f, v_j)_j$ it follows

$$\begin{aligned}\int_K f v_j \, d\mathbf{x} &= \int_K (A\nabla \hat{u}_j \cdot \nabla v_j + (\mu - \nabla \cdot \boldsymbol{\beta}) \hat{u}_j v_j - \hat{u}_j \boldsymbol{\beta} \cdot \nabla v_j) \, d\mathbf{x} \\ &\quad - \sum_{\sigma \in \mathcal{F}_K} \int_{\sigma} ([v_j] \{A\nabla \hat{u}_j\}_{\omega} \cdot \mathbf{n}_{\sigma} + [\hat{u}_j]_{g_j} \{A\nabla v_j\}_{\omega} \cdot \mathbf{n}_{\sigma}) \, d\mathbf{y} \\ &\quad + \sum_{\sigma \in \mathcal{F}_K} \int_{\sigma} ((\eta_{\sigma} \frac{\gamma_{\sigma}}{h_{\sigma}} + \nu_{\sigma}) [\hat{u}_j]_{g_j} [v_j] + \boldsymbol{\beta} \cdot \mathbf{n}_{\sigma} \{\hat{u}_j\}_{g_j} [v_j]) \, d\mathbf{y}.\end{aligned}$$

Since $\{A\nabla v_j\}_{\omega} = \omega_{K,\sigma} A|_K \nabla v_j$ and $[v_j] \mathbf{n}_{\sigma} = v_j|_K \mathbf{n}_K$, using (4.2) and (4.3), we obtain

$$\int_K f v_j \, d\mathbf{x} = \int_K (\nabla \cdot \hat{\mathbf{t}}_j + \nabla \cdot \hat{\mathbf{q}}_j + (\mu - \nabla \cdot \boldsymbol{\beta}) \hat{u}_j) v_j \, d\mathbf{x}\tag{4.4}$$

and the result follows from $\nabla \cdot \hat{\mathbf{t}}_j, \nabla \cdot \hat{\mathbf{q}}_j \in \mathbb{P}_{\sharp}(K)$, $\mathbf{t}_k|_K = \hat{\mathbf{t}}_j|_K$, $\mathbf{q}_k|_K = \hat{\mathbf{q}}_j|_K$ and $u_k|_K = \hat{u}_j|_K$. \square

In order to define the $H_0^1(\Omega)$ conforming approximation s_k of u_k we will need the so-called Oswald operator already considered in [20] for a posteriori estimates. Let $\mathfrak{T} = (D, \mathcal{M}, \mathcal{F})$, $g \in C^0(\partial D)$ and consider $\mathcal{O}_{\mathfrak{T},g} : V(\mathfrak{T}) \rightarrow V(\mathfrak{T}) \cap H^1(D)$, for a function $v \in V(\mathfrak{T})$ the value of $\mathcal{O}_{\mathfrak{T},g}v$ is prescribed at the Lagrange interpolation nodes p of the conforming finite element space $V(\mathfrak{T}) \cap H^1(D)$. Let $p \in D$ be a Lagrange node, if $p \notin \partial D$ we set

$$\mathcal{O}_{\mathfrak{T},g}v(p) = \frac{1}{\#\mathcal{M}_p} \sum_{K \in \mathcal{M}_p} v|_K(p),$$

where $\mathcal{M}_p = \{K \in \mathcal{M} : p \in \overline{K}\}$. If instead $p \in \partial D$ then $\mathcal{O}_{\mathfrak{T},g}v(p) = g(p)$, where g is the Dirichlet condition on ∂D . The reconstructed potential $s_k \in V(\mathfrak{T}_k) \cap H_0^1(\Omega)$ is built as in (3.2), where

$$\hat{s}_k = \mathcal{O}_{\hat{\mathfrak{T}}_k, s_{k-1}} \hat{u}_k. \quad (4.5)$$

4.2 Constants definition and preliminary results

Here we define the constants appearing in (3.4a) to (3.4j) and derive preliminary results needed to prove Theorems 3.1 and 3.2.

Let $K \in \mathcal{M}_k$ and $\sigma \in \mathcal{F}_K$, we recall that $|K|$ is the measure of K and $|\sigma|$ the $d-1$ dimensional measure of σ . We denote by $c_{A,K}$ the minimal eigenvalue of $A|_K$. Next, we denote by $c_{\beta,\mu,K}$ the essential minimum of $\mu - \frac{1}{2}\nabla \cdot \beta \geq 0$ on K . In what follows we will assume that $\mu - \frac{1}{2}\nabla \cdot \beta > 0$ a.e. in Ω , hence $c_{\beta,\mu,K} > 0$ for all $K \in \mathcal{M}_k$, and provide error estimators under this assumption. We explain in Section 4.4 how to overcome this limitation slightly modifying the proofs and error estimators.

The cutoff functions m_K, \tilde{m}_K and m_σ are defined by

$$\begin{aligned} m_K &= \min\{C_p^{1/2}h_K c_{A,K}^{-1/2}, c_{\beta,\mu,K}^{-1/2}\}, \\ \tilde{m}_K &= \min\{(C_p + C_p^{1/2})h_K c_{A,K}^{-1}, h_K^{-1}c_{\beta,\mu,K}^{-1} + c_{\beta,\mu,K}^{-1/2}c_{A,K}^{-1/2}/2\}, \\ m_\sigma^2 &= \min\{\max_{K \in \mathcal{M}_\sigma} \{3d|\sigma|h_K^2|K|^{-1}c_{A,K}^{-1}\}, \max_{K \in \mathcal{M}_\sigma} \{|\sigma||K|^{-1}c_{\beta,\mu,K}^{-1}\}\}, \end{aligned}$$

where $C_p = 1/\pi^2$ is an optimal Poincaré constant for convex domains [25]. Let $v \in H^1(\mathcal{M}_k)$, it holds

$$\|v - \pi_0 v\|_{L^2(K)} \leq m_K \|v\|_K \quad \text{for all } K \in \mathcal{M}_k, \quad (4.7a)$$

$$\|v - \pi_0 v|_K\|_{L^2(\sigma)} \leq C_{t,K,\sigma}^{1/2} \tilde{m}_K^{1/2} \|v\|_K \quad \text{for all } \sigma \in \mathcal{F}_k \text{ and } K \in \mathcal{M}_\sigma, \quad (4.7b)$$

$$\|[\pi_0 v]\|_{L^2(\sigma)} \leq m_\sigma \sum_{K \in \mathcal{M}_\sigma} \|v\|_K \quad \text{for all } \sigma \in \mathcal{F}_k, \quad (4.7c)$$

where $\mathcal{M}_\sigma = \{K \in \mathcal{M}_k : \sigma \subset \partial K\}$ and $C_{t,K,\sigma}$ is the constant of the trace inequality

$$\|v|_K\|_{L^2(\sigma)}^2 \leq C_{t,K,\sigma} (h_K^{-1} \|v\|_{L^2(K)}^2 + \|v\|_{L^2(K)} \|\nabla v\|_{L^2(K)^d}). \quad (4.8)$$

It has been proved in [28, Lemma 3.12] that for a simplex it holds $C_{t,K,\sigma} = |\sigma|h_K/|K|$.

Let us briefly explain the role of constants (4.6) and how the bounds (4.7) are obtained. We observe that for each bound in (4.7) the cut off functions take the minimum between two possible values, allowing for robust error estimation in singularly perturbed regimes. For (4.7a), using the Poincaré inequality [25, equation 3.2] we have

$$\begin{aligned} \|v - \pi_0 v\|_{L^2(K)} &\leq C_p^{1/2} h_K \|\nabla v\|_{L^2(K)^d} \\ &\leq C_p^{1/2} h_K c_{A,K}^{-1/2} \|A^{1/2} \nabla v\|_{L^2(K)^d} \leq C_p^{1/2} h_K c_{A,K}^{-1/2} \|v\|_K. \end{aligned} \quad (4.9a)$$

Denoting $(\cdot, \cdot)_K$ the $L^2(K)$ inner product, it holds

$$\|v - \pi_0 v\|_{L^2(K)}^2 = (v - \pi_0 v, v - \pi_0 v)_K = (v - \pi_0 v, v)_K \leq \|v - \pi_0 v\|_{L^2(K)} \|v\|_{L^2(K)},$$

hence

$$\|v - \pi_0 v\|_{L^2(K)} \leq \|v\|_{L^2(K)} \leq c_{\beta, \mu, K}^{-1/2} \left\| \left(\mu - \frac{1}{2} \nabla \cdot \beta \right)^{1/2} v \right\|_{L^2(K)} \leq c_{\beta, \mu, K}^{-1/2} \|v\|_K \quad (4.9b)$$

and (4.7a) follows. The choice between bounds (4.9a) and (4.9b) depends on whether the problem is singularly perturbed or not. Bounds (4.7b) and (4.7c) are obtained similarly, see [11, Lemma 4.2] and [30, Lemma 4.5]. Finally, for $K \in \mathcal{M}_k$ and $\sigma \in \mathcal{F}_K$ we define

$$D_{t, K, \sigma} = \left(\frac{C_{t, K, \sigma}}{2h_K c_{\beta, \mu, K}} \left(1 + \sqrt{1 + h_K^2 \frac{c_{\beta, \mu, K}}{c_{A, K}}} \right) \right)^{1/2}, \quad (4.10)$$

which is used to bound $\|v|_K\|_{L^2(\sigma)}$ in terms of $\|v\|_K$ in the next lemma.

Lemma 4.3. *Let $v_k \in H^1(\mathcal{M}_k)$, for each $K \in \mathcal{M}_k$ and $\sigma \in \mathcal{F}_K$ it holds*

$$\|v_k|_K\|_{L^2(\sigma)} \leq D_{t, K, \sigma} \|v_k\|_K.$$

Proof. Let $v_k \in H^1(\mathcal{M}_k)$ and $\epsilon > 0$. Applying Hölder inequality to the trace inequality (4.8) we get

$$\|v_k|_K\|_{L^2(\sigma)}^2 \leq C_{t, K, \sigma} \left(h_K^{-1} + \frac{1}{2\epsilon} \right) \|v_k\|_{L^2(K)}^2 + \frac{\epsilon}{2} \|\nabla v_k\|_{L^2(K)^d}^2.$$

Hence, if there exists $D_{t, K, \sigma} > 0$ independent of v_k such that

$$\begin{aligned} C_{t, K, \sigma} \left(h_K^{-1} + \frac{1}{2\epsilon} \right) \|v_k\|_{L^2(K)}^2 + \frac{\epsilon}{2} \|\nabla v_k\|_{L^2(K)^d}^2 \\ \leq D_{t, K, \sigma}^2 (c_{A, K} \|\nabla v_k\|_{L^2(K)^d}^2 + c_{\beta, \mu, K} \|v_k\|_{L^2(K)}^2) \end{aligned} \quad (4.11)$$

then $\|v_k|_K\|_{L^2(\sigma)}^2 \leq D_{t, K, \sigma}^2 \|v_k\|_K^2$ and the result holds. Relation (4.11) holds if

$$C_{t, K, \sigma} \left(h_K^{-1} + \frac{1}{2\epsilon} \right) \leq D_{t, K, \sigma}^2 c_{\beta, \mu, K}, \quad C_{t, K, \sigma} \frac{\epsilon}{2} \leq D_{t, K, \sigma}^2 c_{A, K}$$

and hence $D_{t, K, \sigma}^2 = \max\{C_{t, K, \sigma} (h_K^{-1} + \frac{1}{2\epsilon}) c_{\beta, \mu, K}^{-1}, C_{t, K, \sigma} \frac{\epsilon}{2} c_{A, K}^{-1}\}$. Taking ϵ such that the maximum is minimized we get $D_{t, K, \sigma}$ as in (4.10). \square

The proof of the following Lemma is inspired from [17, Theorem 3.1], the main difference is that we take into account the weaker regularity of the reconstructed fluxes.

Lemma 4.4. *Let $u \in H_0^1(\Omega)$ be the solution to (2.1), $u_k \in V(\mathfrak{T}_k)$ given by Algorithm 1, $s_k \in H_0^1(\Omega)$ from (3.2) and (4.5), $\mathbf{t}_k, \mathbf{q}_k \in H_{\text{div}}(\mathcal{G}_k)$ defined by (3.1) and (4.2) and $v \in H_0^1(\Omega)$. Then*

$$|\mathcal{B}(u - u_k, v) + \mathcal{B}_A(u_k - s_k, v)| \leq \left(\sum_{K \in \mathcal{M}_k} \eta_{1, K}^2 \right)^{1/2} \|v\|,$$

with $\eta_{1, K} = \eta_{R, K} + \eta_{DF, K} + \eta_{C, 1, K} + \eta_{C, 2, K} + \eta_{U, K} + \eta_{\Gamma, 1, K} + \eta_{\Gamma, 2, K}$.

Proof. Since u satisfies (2.1), using the definition of \mathcal{B} and \mathcal{B}_A

$$\begin{aligned} \mathcal{B}(u - u_k, v) + \mathcal{B}_A(u_k - s_k, v) &= \int_{\Omega} (f - (\mu - \nabla \cdot \boldsymbol{\beta})u_k)v \, d\mathbf{x} - \int_{\Omega} A\nabla u_k \cdot \nabla v \, d\mathbf{x} \\ &\quad - \int_{\Omega} \frac{1}{2}(\nabla \cdot \boldsymbol{\beta})(u_k - s_k)v \, d\mathbf{x} - \int_{\Omega} \nabla \cdot (\boldsymbol{\beta}s_k)v \, d\mathbf{x}. \end{aligned}$$

Using $v\mathbf{t}_k \in H_{\text{div}}(\mathcal{G}_k)$, from the divergence theorem we have

$$\begin{aligned} \int_{\Omega} (v\nabla \cdot \mathbf{t}_k + \nabla v \cdot \mathbf{t}_k) \, d\mathbf{x} &= \sum_{G \in \mathcal{G}_k} \int_G \nabla \cdot (v\mathbf{t}_k) \, d\mathbf{x} = \sum_{G \in \mathcal{G}_k} \int_{\partial G} v\mathbf{t}_k \cdot \mathbf{n}_{\partial G} \, d\mathbf{y} \\ &= \sum_{\gamma \in \Gamma_k} \int_{\gamma} \llbracket v\mathbf{t}_k \rrbracket \cdot \mathbf{n}_{\gamma} \, d\mathbf{y} = \sum_{\gamma \in \Gamma_k} \int_{\gamma} \llbracket \mathbf{t}_k \rrbracket \cdot \mathbf{n}_{\gamma} v \, d\mathbf{y} \end{aligned}$$

and hence

$$\begin{aligned} \mathcal{B}(u - u_k, v) + \mathcal{B}_A(u_k - s_k, v) &= \int_{\Omega} (f - \nabla \cdot \mathbf{t}_k - \nabla \cdot \mathbf{q}_k - (\mu - \nabla \cdot \boldsymbol{\beta})u_k)v \, d\mathbf{x} \\ &\quad - \int_{\Omega} \frac{1}{2}(\nabla \cdot \boldsymbol{\beta})(u_k - s_k)v \, d\mathbf{x} + \int_{\Omega} \nabla \cdot (\mathbf{q}_k - \boldsymbol{\beta}s_k)v \, d\mathbf{x} \quad (4.12) \\ &\quad - \int_{\Omega} (A\nabla u_k + \mathbf{t}_k) \cdot \nabla v \, d\mathbf{x} + \sum_{\gamma \in \Gamma_k} \int_{\gamma} \llbracket \mathbf{t}_k \rrbracket \cdot \mathbf{n}_{\gamma} v \, d\mathbf{y}. \end{aligned}$$

From Lemma 4.2 we deduce

$$\begin{aligned} &\left| \int_{\Omega} (f - \nabla \cdot \mathbf{t}_k - \nabla \cdot \mathbf{q}_k - (\mu - \nabla \cdot \boldsymbol{\beta})u_k)v \, d\mathbf{x} \right| \\ &= \left| \int_{\Omega} (f - \nabla \cdot \mathbf{t}_k - \nabla \cdot \mathbf{q}_k - (\mu - \nabla \cdot \boldsymbol{\beta})u_k)(v - \pi_0 v) \, d\mathbf{x} \right| \quad (4.13a) \\ &\leq \sum_{K \in \mathcal{M}_k} \eta_{R,K} \|v\|_K. \end{aligned}$$

Similarly, we get

$$\begin{aligned} \left| \int_{\Omega} (A\nabla u_k + \mathbf{t}_k) \cdot \nabla v \, d\mathbf{x} \right| &\leq \sum_{K \in \mathcal{M}_k} \eta_{DF,K} \|v\|_K, \\ \left| \int_{\Omega} \frac{1}{2}(\nabla \cdot \boldsymbol{\beta})(u_k - s_k)v \, d\mathbf{x} \right| &\leq \sum_{K \in \mathcal{M}_k} \eta_{C,2,K} \|v\|_K. \end{aligned} \quad (4.13b)$$

Since $\llbracket \mathbf{t}_k \rrbracket_{\sigma} = 0$ for $\sigma \in \mathcal{F}_{k,i} \setminus \cup_{\gamma \in \Gamma_k} \mathcal{F}_{\gamma}$, it holds

$$\sum_{\gamma \in \Gamma_k} \int_{\gamma} \llbracket \mathbf{t}_k \rrbracket \cdot \mathbf{n}_{\gamma} v \, d\mathbf{y} = \sum_{\sigma \in \mathcal{F}_{k,i}} \int_{\sigma} \llbracket \mathbf{t}_k \rrbracket \cdot \mathbf{n}_{\sigma} v \, d\mathbf{y} = \frac{1}{2} \sum_{K \in \mathcal{M}_k} \sum_{\sigma \in \mathcal{F}_K \cap \mathcal{F}_{k,i}} \int_{\sigma} \llbracket \mathbf{t}_k \rrbracket \cdot \mathbf{n}_{\sigma} v \, d\mathbf{y}.$$

Using Lemma 4.3 we obtain

$$\begin{aligned} \left| \sum_{\gamma \in \Gamma_k} \int_{\gamma} \llbracket \mathbf{t}_k \rrbracket \cdot \mathbf{n}_{\gamma} v \, d\mathbf{y} \right| &\leq \frac{1}{2} \sum_{K \in \mathcal{M}_k} \sum_{\sigma \in \mathcal{F}_K \cap \mathcal{F}_{k,i}} \|\llbracket \mathbf{t}_k \rrbracket \cdot \mathbf{n}_{\sigma}\|_{L^2(\sigma)} \|v\|_{L^2(\sigma)} \\ &\leq \sum_{K \in \mathcal{M}_k} \eta_{\Gamma,2,K} \|v\|_K. \end{aligned} \quad (4.13c)$$

It remains to estimate $\int_{\Omega} \nabla \cdot (\mathbf{q}_k - \boldsymbol{\beta}s_k)v \, d\mathbf{x}$. For that, we use

$$\begin{aligned} \int_{\Omega} \nabla \cdot (\mathbf{q}_k - \boldsymbol{\beta}s_k)v \, d\mathbf{x} &= \sum_{K \in \mathcal{M}_k} \int_K (\mathcal{I} - \pi_0) \nabla \cdot (\mathbf{q}_k - \boldsymbol{\beta}s_k)(v - \pi_0 v) \, d\mathbf{x} \\ &\quad + \sum_{K \in \mathcal{M}_k} \sum_{\sigma \in \mathcal{F}_K} \int_{\sigma} (\mathbf{q}_k - \boldsymbol{\beta}s_k) \cdot \mathbf{n}_K \pi_0 v \, d\mathbf{y} \end{aligned}$$

and from (4.7a) we get

$$\left| \sum_{K \in \mathcal{M}_k} \int_K (\mathcal{I} - \pi_0) \nabla \cdot (\mathbf{q}_k - \boldsymbol{\beta}s_k)(v - \pi_0 v) \, d\mathbf{x} \right| \leq \sum_{K \in \mathcal{M}_k} \eta_{C,1,K} \|v\|_K. \quad (4.13d)$$

For the second term we write

$$\begin{aligned} \sum_{K \in \mathcal{M}_k} \sum_{\sigma \in \mathcal{F}_K} \int_{\sigma} (\mathbf{q}_k - \boldsymbol{\beta}s_k) \cdot \mathbf{n}_K \pi_0 v \, d\mathbf{y} &= \sum_{\sigma \in \mathcal{F}_k} \int_{\sigma} [\pi_{0,\sigma}(\mathbf{q}_k - \boldsymbol{\beta}s_k) \pi_0 v] \cdot \mathbf{n}_{\sigma} \, d\mathbf{y} \\ &= \sum_{\sigma \in \mathcal{F}_{k,i}} \int_{\sigma} \{\pi_0 v\} [\pi_{0,\sigma}(\mathbf{q}_k - \boldsymbol{\beta}s_k)] \cdot \mathbf{n}_{\sigma} + [\pi_0 v] \{\pi_{0,\sigma}(\mathbf{q}_k - \boldsymbol{\beta}s_k)\} \cdot \mathbf{n}_{\sigma} \, d\mathbf{y} \\ &\quad + \sum_{\sigma \in \mathcal{F}_{k,b}} \int_{\sigma} \pi_0 v \pi_{0,\sigma}(\mathbf{q}_k - \boldsymbol{\beta}s_k) \cdot \mathbf{n}_{\sigma} \, d\mathbf{y} = \text{I} + \text{II} + \text{III} \end{aligned}$$

and we easily obtain, since $[\boldsymbol{\beta}s_k] = 0$,

$$\text{I} = \frac{1}{2} \sum_{K \in \mathcal{M}_k} \sum_{\sigma \in \mathcal{F}_K \cap \mathcal{F}_{k,i}} \int_{\sigma} \pi_0 v|_K [\pi_{0,\sigma} \mathbf{q}_k] \cdot \mathbf{n}_{\sigma} \, d\mathbf{y}.$$

Using $|\pi_0 v|_K| = |K|^{-1/2} \|\pi_0 v\|_{L^2(K)} \leq |K|^{-1/2} \|v\|_{L^2(K)} \leq (|K|c_{\boldsymbol{\beta},\mu,K})^{-1/2} \|v\|_K$ we get

$$\text{I} \leq \frac{1}{2} \sum_{K \in \mathcal{M}_k} \sum_{\sigma \in \mathcal{F}_K \cap \mathcal{F}_{k,i}} (|K|c_{\boldsymbol{\beta},\mu,K})^{-1/2} \|[\pi_{0,\sigma} \mathbf{q}_k] \cdot \mathbf{n}_{\sigma}\|_{L^1(\sigma)} \|v\|_K = \sum_{K \in \mathcal{M}_k} \eta_{\Gamma,1,K} \|v\|_K. \quad (4.13e)$$

Let $\mathcal{M}_{\sigma} = \{K \in \mathcal{M}_k : \sigma \subset \partial K\}$, using (4.7c) for the second term we have

$$\begin{aligned} \text{II} &\leq \sum_{\sigma \in \mathcal{F}_{k,i}} m_{\sigma} \|\pi_{0,\sigma} \{\mathbf{q}_k - \boldsymbol{\beta}s_k\} \cdot \mathbf{n}_{\sigma}\|_{L^2(\sigma)} \sum_{K \in \mathcal{M}_{\sigma}} \|v\|_K \\ &= \sum_{K \in \mathcal{M}_k} \sum_{\sigma \in \mathcal{F}_K \cap \mathcal{F}_{k,i}} m_{\sigma} \|\pi_{0,\sigma} \{\mathbf{q}_k - \boldsymbol{\beta}s_k\} \cdot \mathbf{n}_{\sigma}\|_{L^2(\sigma)} \|v\|_K. \end{aligned}$$

For the last term we similarly obtain

$$\text{III} \leq \sum_{K \in \mathcal{M}_k} \sum_{\sigma \in \mathcal{F}_K \cap \mathcal{F}_{k,b}} m_{\sigma} \|\pi_{0,\sigma}(\mathbf{q}_k - \boldsymbol{\beta}s_k) \cdot \mathbf{n}_{\sigma}\|_{L^2(\sigma)} \|v\|_K$$

and hence

$$\text{II} + \text{III} \leq \sum_{K \in \mathcal{M}_k} \sum_{\sigma \in \mathcal{F}_K} \chi_{\sigma} m_{\sigma} \|\pi_{0,\sigma} \{\mathbf{q}_k - \boldsymbol{\beta}s_k\} \cdot \mathbf{n}_{\sigma}\|_{L^2(\sigma)} \|v\|_K = \sum_{K \in \mathcal{M}_k} \eta_{U,K} \|v\|_K, \quad (4.13f)$$

where $\chi_{\sigma} = 2$ if $\sigma \in \mathcal{F}_{k,b}$ and $\chi_{\sigma} = 1$ if $\sigma \in \mathcal{F}_{k,i}$. Plugging relations (4.13a) to (4.13f) into (4.12) we get the result. \square

In Lemma 4.4 we use Lemma 4.2 to deduce that

$$\int_K (\nabla \cdot \mathbf{t}_k + \nabla \cdot \mathbf{q}_k + (\mu - \nabla \cdot \boldsymbol{\beta})u_k) \, d\mathbf{x} = \int_K f \, d\mathbf{x} \quad (4.14)$$

and hence (4.13a). However, when the mesh has hanging nodes inside of the local domains Lemma 4.2 is not valid. Indeed, if $\widehat{\mathcal{M}}_k$ has hanging nodes, the fluxes $\hat{\mathbf{t}}_k, \hat{\mathbf{q}}_k$ must be constructed on a matching (free of hanging nodes) submesh $\overline{\mathcal{M}}_k$ of $\widehat{\mathcal{M}}_k$, otherwise they may fail to be in $H_{\text{div}}(\Omega_k)$. The constructed fluxes will satisfy relation (4.4), but since $\nabla \cdot \hat{\mathbf{t}}_k, \nabla \cdot \hat{\mathbf{q}}_k \in \mathbb{P}_2(K')$ for $K' \in \overline{\mathcal{M}}_k$ and $\overline{\mathcal{M}}_k$ is finer than $\widehat{\mathcal{M}}_k$, then we cannot conclude as we did in Lemma 4.2. Nonetheless, (4.4) still implies (4.14), which is enough to prove Lemma 4.4.

4.3 Proof of the theorems

Here we prove Theorems 3.1 and 3.2. We will consider $\mathcal{B} : H_0^1(\Omega) \times H_0^1(\Omega) \rightarrow \mathbb{R}$ defined in (2.2) for functions in $H^1(\mathcal{M}_k)$.

Proof of Theorem 3.1. It has been proved in [16, Lemma 3.1] that for any $u_k \in V(\mathfrak{T}_k)$ and $u, s \in H_0^1(\Omega)$ it holds

$$\|u - u_k\| \leq \|u_k - s\| + |\mathcal{B}(u - u_k, v) + \mathcal{B}_A(u_k - s, v)|,$$

with $v = (u - s)/\|u - s\|$. Choosing u as the exact solution to (2.1), u_k given by Algorithm 1, $s = s_k$ from (3.2) and using Lemma 4.4 gives the result. \square

Proof of Theorem 3.2. Since $u \in H_0^1(\Omega)$ it holds $\mathcal{B}_J(u, w) = 0$ for all $w \in H_0^1(\Omega)$, using $\mathcal{B}_A \leq \mathcal{B} + |\mathcal{B}_S|$ we get

$$\|u - u_k\|_{\oplus} \leq 2\|u - u_k\| + \sup_{\substack{w \in H_0^1(\Omega) \\ \|w\|=1}} (\mathcal{B}(u - u_k, w) - \mathcal{B}_J(u_k, w)).$$

To conclude the proof we show that

$$\sup_{\substack{w \in H_0^1(\Omega) \\ \|w\|=1}} (\mathcal{B}(u - u_k, w) - \mathcal{B}_J(u_k, w)) \leq \left(\sum_{K \in \mathcal{M}_k} \eta_{2,K}^2 \right)^{1/2}.$$

Following Lemma 4.4, we easily get

$$\begin{aligned} \mathcal{B}(u - u_k, w) - \mathcal{B}_J(u_k, w) &\leq \sum_{K \in \mathcal{M}_k} (\eta_{R,K} + \eta_{DF,K} + \tilde{\eta}_{C,1,K} + \eta_{\Gamma,2,K}) \|w\|_K \\ &\quad + \sum_{K \in \mathcal{M}_k} \sum_{\sigma \in \mathcal{F}_K} \int_{\sigma} \pi_0 w (\mathbf{q}_k - \boldsymbol{\beta} u_k) \cdot \mathbf{n}_K \, d\mathbf{y} - \mathcal{B}_J(u_k, w). \end{aligned}$$

The two last terms satisfy

$$\begin{aligned} &\sum_{\sigma \in \mathcal{F}_k} \int_{\sigma} [\pi_0 w (\mathbf{q}_k - \boldsymbol{\beta} u_k)] \cdot \mathbf{n}_{\sigma} \, d\mathbf{y} - \mathcal{B}_J(u_k, w) \\ &= \sum_{\sigma \in \mathcal{F}_k} \chi_{\sigma} \int_{\sigma} [\pi_0 w] \pi_{0,\sigma} \{\mathbf{q}_k - \boldsymbol{\beta} u_k\} \cdot \mathbf{n}_{\sigma} \, d\mathbf{y} + \sum_{\sigma \in \mathcal{F}_{k,i}} \int_{\sigma} \{\pi_0 w\} [\pi_{0,\sigma} \mathbf{q}_k] \cdot \mathbf{n}_{\sigma} \, d\mathbf{y} \\ &\leq \sum_{K \in \mathcal{M}_k} (\tilde{\eta}_{U,K} + \eta_{\Gamma,1,K}) \|w\|_K, \end{aligned}$$

where in the last step we followed again Lemma 4.4. \square

4.4 Alternative error bounds

Our aim here is to explain how to avoid the assumption $c_{\beta,\mu,K} > 0$ for all $K \in \mathcal{M}_k$ made in Sections 3.1 and 4.2. This assumption is needed to define $\eta_{\Gamma,1,K}$, $\eta_{\Gamma,2,K}$ but can be avoided if (4.13c) and (4.13e) are estimated differently. For (4.13c), using the trace inequality (4.8) we get

$$\begin{aligned} \left| \sum_{\gamma \in \Gamma_k} \int_{\gamma} \llbracket \mathbf{t}_k \rrbracket \cdot \mathbf{n}_{\gamma} v \, d\mathbf{y} \right| &\leq \frac{1}{2} \sum_{K \in \mathcal{M}_k} \sum_{\sigma \in \mathcal{F}_K \cap \mathcal{F}_{k,i}} \|\llbracket \mathbf{t}_k \rrbracket \cdot \mathbf{n}_{\sigma}\|_{L^2(\sigma)} \|v|_K\|_{L^2(\sigma)} \\ &\leq \sum_{K \in \mathcal{M}_k} \tilde{\eta}_{\Gamma,2,K} (\|v\|_{L^2(K)}^2 + h_K \|v\|_{L^2(K)} \|\nabla v\|_{L^2(K)^d})^{1/2}, \end{aligned}$$

where

$$\tilde{\eta}_{\Gamma,2,K} = \frac{1}{2} \sum_{\sigma \in \mathcal{F}_K \cap \mathcal{F}_{k,i}} h_K^{-1/2} C_{t,K,\sigma}^{1/2} \|\llbracket \mathbf{t}_k \rrbracket \cdot \mathbf{n}_{\sigma}\|_{L^2(\sigma)}.$$

Setting $\tilde{\eta}_{\Gamma,2}^2 = \sum_{K \in \mathcal{M}_k} \tilde{\eta}_{\Gamma,2,K}^2$, it yields

$$\begin{aligned} \left| \sum_{\gamma \in \Gamma_k} \int_{\gamma} \llbracket \mathbf{t}_k \rrbracket \cdot \mathbf{n}_{\gamma} v \, d\mathbf{y} \right| &\leq \tilde{\eta}_{\Gamma,2} \left(\sum_{K \in \mathcal{M}_k} \|v\|_{L^2(K)}^2 + h_K \|v\|_{L^2(K)} \|\nabla v\|_{L^2(K)^d} \right)^{1/2} \\ &\leq \tilde{\eta}_{\Gamma,2} \left(\|v\|_{L^2(\Omega)}^2 + h_{\mathcal{M}_k} \|v\|_{L^2(\Omega)} \|\nabla v\|_{L^2(\Omega)^d} \right)^{1/2}. \end{aligned}$$

Using the Poincaré inequality $\|v\|_{L^2(\Omega)} \leq d_{\Omega} \|\nabla v\|_{L^2(\Omega)^d}$, where d_{Ω} is the diameter of Ω , we get

$$\left| \sum_{\gamma \in \Gamma_k} \int_{\gamma} \llbracket \mathbf{t}_k \rrbracket \cdot \mathbf{n}_{\gamma} v \, d\mathbf{y} \right| \leq \tilde{\eta}_{\Gamma,2} \left(d_{\Omega}^2 + h_{\mathcal{M}_k} d_{\Omega} \right)^{1/2} \|\nabla v\|_{L^2(\Omega)^d} \leq \tilde{\eta}_{\Gamma,2} c_A^{-1/2} \left(d_{\Omega}^2 + h_{\mathcal{M}_k} d_{\Omega} \right)^{1/2} \|v\|,$$

where c_A is the minimal eigenvalue of $A(\mathbf{x})$ over Ω . The same procedure can be used to replace (4.13e) by a relation avoiding the term $c_{\beta,\mu,K}^{-1/2}$. The new bounds can be used to modify the results of Theorems 3.1 and 3.2 and obtain error estimators when $\mu - \frac{1}{2} \nabla \cdot \beta > 0$ is not satisfied.

5 Numerical Experiments

In order to study the properties and illustrate the performance of the local scheme we consider here several numerical examples. First, in Section 5.1, we look at the convergence rates of the error estimators, focusing on the errors introduced by solving only local problems. Considering a local and a nonlocal problem, we also compare the size of the new error estimators $\eta_{\Gamma,1}$ and $\eta_{\Gamma,2}$ against the classical terms. We emphasize that we do not use the automatic subdomains' identification algorithm for this example, as the subdomains are fixed beforehand. We also perform in Section 5.2 an experiment for a smooth problem, where the errors are not localized, illustrating the role of $\eta_{\Gamma,1}$ and $\eta_{\Gamma,2}$. To do so, we also compare the local scheme against a classical adaptive method, where after each mesh refinement the problem is solved again on the whole domain. The classical method we refer to is given by Algorithm 2. Second, we investigate the efficiency of the new local algorithm for non smooth problems in Sections 5.3 and 5.4. For such examples, that are the target of our method, the local scheme performs better than the classical one. We conclude in Section 5.5 with a

Algorithm 2 ClassicalScheme(\mathfrak{T}_1)

Find $\bar{u}_1 \in V(\mathfrak{T}_1)$ solution to $\mathcal{B}(\bar{u}_1, v_1, \mathfrak{T}_1, 0) = (f, v_1)_1$ for all $v_1 \in V(\mathfrak{T}_1)$.
for $k = 2, \dots, M$ **do**
 $(\mathfrak{T}_k, \widehat{\mathfrak{T}}_k) = \text{LocalDomain}(\bar{u}_{k-1}, \mathfrak{T}_{k-1})$.
 Find $\bar{u}_k \in V(\mathfrak{T}_k)$ solution to $\mathcal{B}(\bar{u}_k, v_k, \mathfrak{T}_k, 0) = (f, v_k)_1$ for all $v_k \in V(\mathfrak{T}_k)$.
end for

nonlinear problem, where Theorems 3.1 and 3.2 do not apply but Algorithm 1 can nevertheless be employed in conjunction with a Newton scheme.

In all the experiments we use \mathbb{P}_1 elements ($\ell = 1$ in (2.3)) on a simplicial mesh with penalization parameter $\eta_\sigma = 10$, the diffusive and convective fluxes $\mathbf{t}_k, \mathbf{q}_k$ are computed with $\mathbf{z} = 0$ (see (4.1)). Furthermore, $\boldsymbol{\beta}$ is always such that $\nabla \cdot \boldsymbol{\beta} = 0$. These choices give $\eta_{C,1,K} = \eta_{C,2,K} = \tilde{\eta}_{C,1,K} = 0$. For an estimator $\eta_{*,K}$ we define $\eta_*^2 = \sum_{K \in \mathcal{M}_k} \eta_{*,K}^2$. Similarly to [17], if $A = \varepsilon I_2$ and $\boldsymbol{\beta}$ is constant then for $v_k \in H^1(\mathcal{M}_k)$ the augmented norm is well estimated by

$$\begin{aligned} \|v_k\|_{\oplus} \leq \|v_k\|_{\oplus'} &= \|v_k\| + \varepsilon^{-1/2} \|\boldsymbol{\beta}\|_2 \|v_k\|_{L^2(\Omega)} \\ &+ \frac{1}{2} \left(\sum_{K \in \mathcal{M}_k} \left(\sum_{\sigma \in \mathcal{F}_K \cap \mathcal{F}_{k,i}} \tilde{m}_K^{1/2} C_{t,K,\sigma}^{1/2} \| [v_k] \boldsymbol{\beta} \cdot \mathbf{n}_\sigma \|_{L^2(\sigma)} \right)^2 \right)^{1/2}. \end{aligned}$$

Hence, in the numerical experiments we consider the computable norm $\| \cdot \|_{\oplus'}$. The effectivity indexes of the error estimators η and $\tilde{\eta}$ from Theorems 3.1 and 3.2 are defined as

$$\frac{\eta}{\|u - u_k\|} \quad \text{and} \quad \frac{\tilde{\eta}}{\|u - u_k\|_{\oplus'}}, \quad (5.1)$$

respectively. For the solution \bar{u}_k of the classical algorithm we use the error estimators η and $\tilde{\eta}$ from [17]. They are equivalent to the estimators presented in this paper except that for \bar{u}_k we have $\eta_{\Gamma,1,K} = \eta_{\Gamma,2,K} = 0$, as in this case the reconstructed fluxes are in $H_{\text{div}}(\Omega)$. The effectivity indexes for \bar{u}_k are as in (5.1) but with u_k replaced by \bar{u}_k . The numerical experiments have been performed with the help of the C++ library `libMesh` [22].

5.1 Problem shifting from localized to nonlocalized errors

We investigate an example in two different locality regimes. First, the errors are confined in a small region and then they are distributed in the whole domain. We will study the effects of this transition on the size of the new error estimators $\eta_{\Gamma,1}$ and $\eta_{\Gamma,2}$.

We solve (1.1) in $\Omega = [0, 1] \times [0, 1]$ with $A = I_2$, $\boldsymbol{\beta} = -(1, 1)^\top$ and $\mu = 1$. The force term f is chosen so that the exact solution reads

$$u(\mathbf{x}) = e^{-\kappa \|\mathbf{x}\|_2} \left(x_1 - \frac{1 - e^{-\kappa x_1}}{1 - e^{-\kappa}} \right) \left(x_2 - \frac{1 - e^{-\kappa x_2}}{1 - e^{-\kappa}} \right), \quad (5.2)$$

with $\kappa = 100$ or $\kappa = 10$. When $\kappa = 100$ the solution has a narrow peak and the errors are localized around that region, when $\kappa = 10$ the solution is smoother and the errors are distributed in the whole domain. See Figures 3(a) and 3(b).

First, we investigate the convergence rate of the error estimators and then we comment on the size of the new error estimators $\eta_{\Gamma,1}$, $\eta_{\Gamma,2}$ when the errors are localized or not, i.e. when $\kappa = 100$

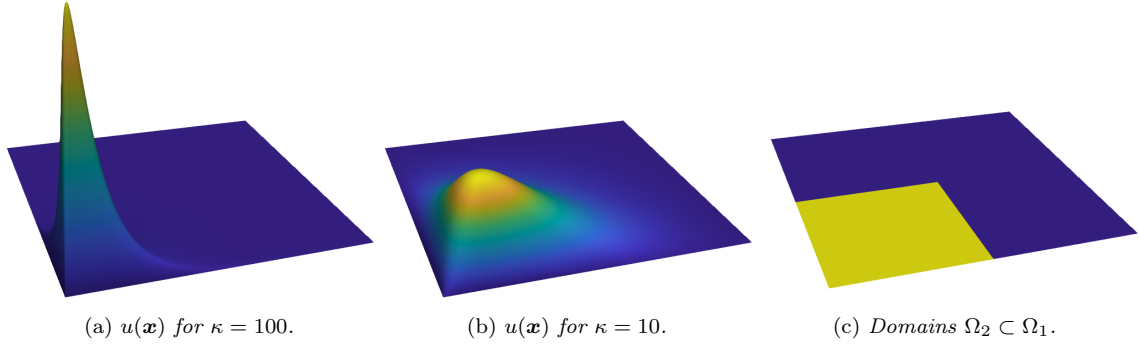


Figure 3. Solution $u(\mathbf{x})$ in (5.2) for two values of κ and local domains Ω_1, Ω_2 .

h	$\ u - u_k\ $	η_{NC}	η_R	η_{DF}	η_U	$\tilde{\eta}_U$	$\eta_{\Gamma,1}$	$\eta_{\Gamma,2}$
2^{-6}	4.2e-1	1.3e-1	1.1e-1	5.7e-1	4.5e-3	2.7e-4	1e-3	1e-1
2^{-7}	2.1e-1	5.8e-2	2.9e-2	2.9e-1	9.1e-4	4.7e-5	8.3e-4	8e-2
2^{-8}	1.1e-1	2.6e-2	7.3e-3	1.4e-1	1.8e-4	8.7e-6	6.2e-4	5.7e-2
2^{-9}	5.3e-2	1.2e-2	1.8e-3	7.1e-2	3.6e-5	2.1e-6	4.5e-4	3.9e-2
Order	1	1	2	1	2	2	0.5	0.5

Table 1. Convergence rate of error estimators for $\kappa = 100$.

or $\kappa = 10$. We define two domains Ω_1, Ω_2 as follows: $\Omega_1 = \Omega$ and $\mathbf{x} \in \Omega_2$ if $\|\mathbf{x}\|_\infty \leq 1/2$, see Figure 3(c). Let h be the grid size of $\widehat{\mathcal{M}}_1$, then the grid size of $\widehat{\mathcal{M}}_2$ is $h/2$. For different choices of h we run Algorithm 1 without calling LocalDomain, since the local domains and meshes are chosen beforehand. After the second iteration we compute the exact energy error and the error estimators. The results are reported in Tables 1 and 2 for $\kappa = 100$ and $\kappa = 10$, respectively. We recall that η_{NC} measures the non conformity of u_k , η_R measures the error in the energy conservation, η_{DF} the difference between $-A\nabla u_k$ and the reconstructed diffusive flux \mathbf{t}_k , $\eta_U, \tilde{\eta}_U$ are upwind errors and $\eta_{\Gamma,1}, \eta_{\Gamma,2}$ measure the jumps of $\mathbf{t}_k, \mathbf{q}_k$ across subdomains boundaries.

We see that the energy error converges with order one, as predicted by the a priori error analysis of [1]. We also observe that the error estimators $\eta_{\Gamma,1}$ and $\eta_{\Gamma,2}$ measuring the reconstructed fluxes' jumps across subdomains' boundaries have a lower rate of convergence. Therefore, the error estimators are not efficient, in the sense that they cannot be bounded from above by the energy error multiplied

h	$\ u - u_k\ $	η_{NC}	η_R	η_{DF}	η_U	$\tilde{\eta}_U$	$\eta_{\Gamma,1}$	$\eta_{\Gamma,2}$
2^{-6}	1.8e-2	4.6e-3	6.3e-4	2.3e-2	3.5e-4	3.2e-4	1e-2	1.8e-1
2^{-7}	9e-3	2.2e-3	1.6e-4	1.2e-2	1.2e-4	1.1e-4	7.2e-3	1.3e-1
2^{-8}	4.5e-3	1.1e-3	3.9e-5	5.8e-3	4.1e-5	4e-5	5.1e-3	8.8e-2
2^{-9}	2.3e-3	5.3e-4	9.9e-6	2.9e-3	1.4e-5	1.4e-5	3.6e-3	6.2e-2
Order	1	1	2	1	1.5	1.5	0.5	0.5

Table 2. Convergence rate of error estimators for $\kappa = 10$.

k	$\ u - u_k\ $	η_{NC}	η_R	η_{DF}	η_U	$\tilde{\eta}_U$	$\eta_{\Gamma,1}$	$\eta_{\Gamma,2}$
1	2.5e-1	9.2e-2	9.6e-2	3.2e-1	4.8e-2	3.8e-3	0	0
2	1.4e-1	5.1e-2	4.8e-2	1.8e-1	1.4e-2	1.7e-3	7.2e-16	6.7e-2
3	9.2e-2	3e-2	3.9e-2	1.2e-1	5.9e-3	1.4e-3	7.5e-4	1.9e-1
4	8.1e-2	2.6e-2	3e-2	1e-1	4.4e-3	1.2e-3	5.9e-4	1.8e-1
5	7.2e-2	2.5e-2	2.5e-2	9.3e-2	4e-3	1.6e-3	1.1e-2	3.4e-1

Table 3. Section 5.2, nonlocal smooth problem. Dominance of $\eta_{\Gamma,1}$ and $\eta_{\Gamma,2}$ over the other error estimators. Only the results of the first five iterations are shown, i.e. $k \leq 5$.

by a mesh-size independent constant. However, the relative size of $\eta_{\Gamma,1}$, $\eta_{\Gamma,2}$ compared to the other estimators gives an information on the suitability of the local scheme:

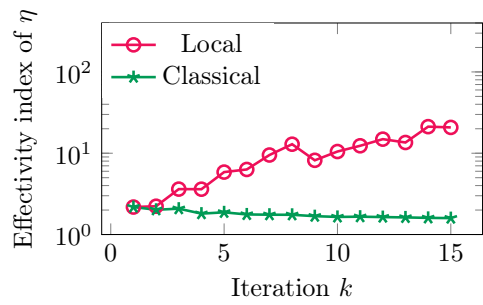
- if $\eta_{\Gamma,1}$, $\eta_{\Gamma,2}$ are comparable to the other estimators one should use the local scheme. The typical situation is when the errors are localized, with local regions covering the large error regions (see Figures 3(a) and 3(c) and Table 1);
- if the relative size of $\eta_{\Gamma,1}$, $\eta_{\Gamma,2}$ is larger than the other estimators, this is an indication that one should switch from local to classical method. The typical situation is when the errors are not (or less) localized (see Figures 3(b) and 3(c) and Table 2). On purpose we did choose a local domain that is too small to cover the error region.

In the next experiments we let the scheme select the local subdomains on the fly, using the fixed energy fraction marking strategy [14, Section 4.2] implemented in the `LocalDomain(u_k, \mathfrak{T}_k)` routine of Algorithm 1. First, we revisit the example of Section 5.1. Second, we consider two examples where the errors are localized, illustrating the efficiency of the algorithm.

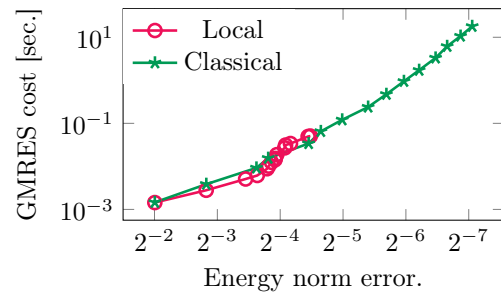
5.2 A nonlocal smooth problem

Considering the same problem as in Section 5.1 with $\kappa = 10$, we run the local and classical schemes for $k = 1, \dots, 15$ starting with a uniform mesh of 128 elements. Here, we employ the automatic subdomains' identification algorithm and the goal is to show when one should switch from local to nonlocal methods. As the error is distributed in the whole domain, it is not possible to chose the subdomains Ω_k so that the errors at their boundaries are negligible. Consequently, the error estimators $\eta_{\Gamma,1}$, $\eta_{\Gamma,2}$ will dominate. Indeed, we see in Table 3 that the error estimators $\eta_{\Gamma,1}$, $\eta_{\Gamma,2}$ measuring the reconstructed fluxes' jumps dominate the other estimators. This phenomenon brings two issues into the algorithm. First, the effectivity index of the local scheme is significantly larger than the index for the classical scheme, as we illustrate in Figure 4(a). Second, the marking error estimator $\eta_{M,K}$ (3.5) will be larger at the boundaries of the local domains than in the large error regions; indeed, we see in Figure 5 that the local domain Ω_4 chosen by the algorithm do not correspond to a large error region but is in a neighborhood of the boundary of Ω_3 , where $\eta_{\Gamma,1}$, $\eta_{\Gamma,2}$ are large. For this reason the algorithm is unable to detect the high error regions and we see in Figure 4(b), where we show the computational cost in function of the energy errors, that the error of the local method stagnates.

This example shows that if the errors are not localized then the estimators $\eta_{\Gamma,1}$, $\eta_{\Gamma,2}$ dominate, the local scheme becomes inefficient and a classical *global* method should be preferred over a local method. However, our algorithm allows to monitor the size of the error estimators $\eta_{\Gamma,1}$ and $\eta_{\Gamma,2}$ and when these error estimators start to dominate the other error indicators (as seen in Table 3) it provides a switching criteria.



(a) Effectivity index of η .



(b) GMRES cost versus energy norm error.

Figure 4. Section 5.2, nonlocal smooth problem. Effectivity indexes in function of the iteration number.

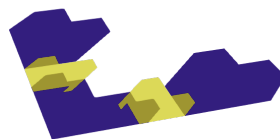


Figure 5. Local domains Ω_3 (darker) and Ω_4 (brighter).

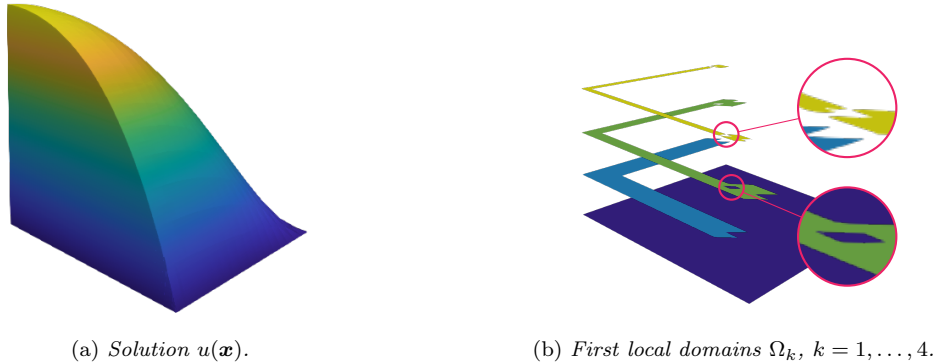


Figure 6. Solution $u(\mathbf{x})$ in (5.3) of the reaction dominated problem and first local domains chosen by the error estimators.

5.3 Reaction dominated problem

In our next example we consider a symmetric problem and want to compare the local and classical schemes (Algorithms 1 and 2) in a singularly perturbed regime. We investigate the efficiency measured as the computational cost and analyze their effectivity indexes. The setting is as follows: we solve (1.1) in $\Omega = [0, 1] \times [0, 1]$ with $\varepsilon = 10^{-6}$, $A = \varepsilon I_2$, $\boldsymbol{\beta} = (0, 0)^\top$, $\mu = 1$ and we choose f such that the exact solution is given by

$$u(\mathbf{x}) = e^{x_1+x_2} \left(x_1 - \frac{1 - e^{-\zeta x_1}}{1 - e^{-\zeta}} \right) \left(x_2 - \frac{1 - e^{-\zeta x_2}}{1 - e^{-\zeta}} \right), \quad (5.3)$$

where $\zeta = 10^4$. The solution is illustrated in Figure 6(a).

Since the problem is symmetric we have $\|\cdot\| = \|\cdot\|_{\oplus}$, but their related error estimators η and $\tilde{\eta}$, respectively, satisfy $\tilde{\eta} > \eta$ and hence the effectivity index of η will be lower (see Theorems 3.1 and 3.2).

Starting from a coarse mesh (128 elements), we let the two algorithms run for $k = 1, \dots, 20$. In Figure 6(b) we show the first four subdomains Ω_k chosen by the local scheme. Note that the local domain Ω_4 chosen by the algorithm is disconnected, while subdomain Ω_3 has a hole; as is allowed by the theory. Several of the subsequent subdomains (not displayed) are also disconnected or contain holes. The first iterations are needed to capture the boundary layer and reach the convergence regime, hence we will plot the results for $k \geq 7$. The most expensive part of the code is the solution of linear systems by means of the conjugate gradient (CG) method preconditioned with the incomplete Cholesky factorization, followed by the computation of the potential and fluxes reconstruction and then by the evaluation of the error estimators. In the local scheme, the time spent doing these tasks is proportional to the number of elements inside each subdomain Ω_k . For the classical scheme, the cost of these tasks depends on the total number of elements in the mesh. Since the CG routine is the most expensive part, we take the time spent in it as an indicator for the computational cost.

In Figure 7(a), we plot the simulation cost against the error estimator η , for both the local and classical algorithms. Each circle or star in the figure represents an iteration k . We observe that the local scheme provides similar error bounds but at a smaller cost. The effectivity index of η at each

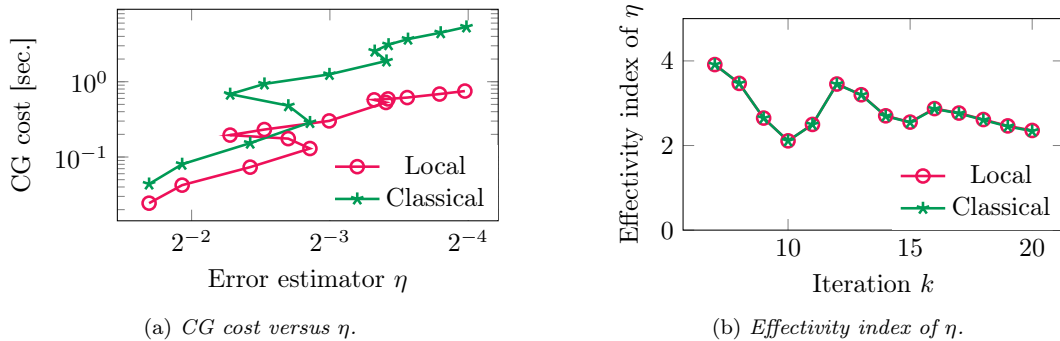


Figure 7. Section 5.3, reaction dominated problem. Computational cost vs. η and effectivity index in function of the iteration number.

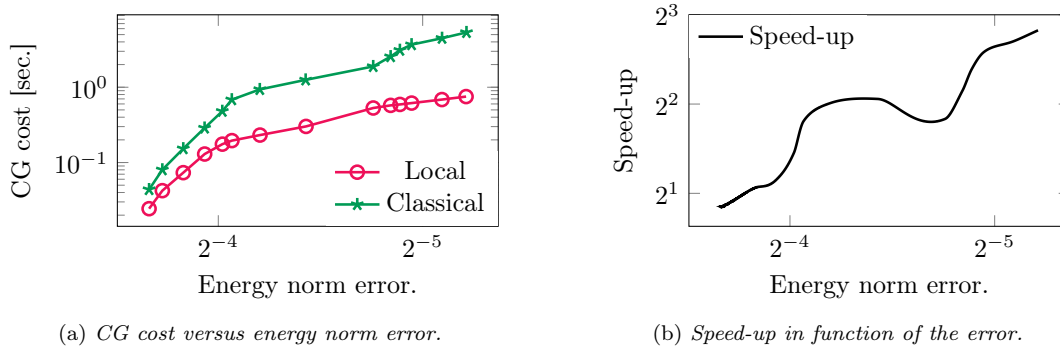


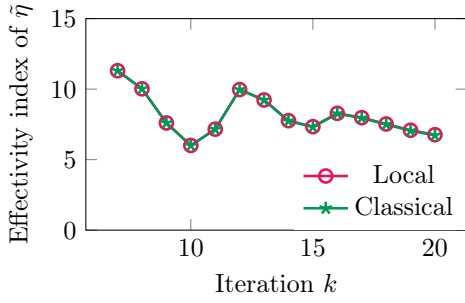
Figure 8. Section 5.3, reaction dominated problem. Computational cost vs. energy norm error and speed-up in function of the error.

iteration k is shown in Figure 7(b), we can observe that the local scheme has an effectivity index similar to the classical scheme.

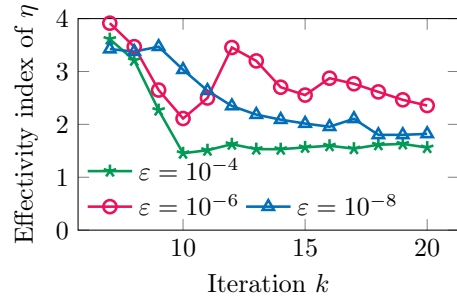
In Figure 8(a) we exhibit the cost against the exact energy error and we notice that for some values of k the mesh is refined but the error stays almost constant. This phenomenon significantly increases the simulation cost of the classical scheme without improving the solution. In contrast, the cost of the local scheme increases only marginally. Dividing the two curves in Figure 8(a) we obtain the relative speed-up, which is plotted in Figure 8(b). We note that as the error decreases the local scheme becomes faster than the classical scheme. In Figure 9(a) we plot the effectivity index of $\tilde{\eta}$. As expected, for this symmetric problem, it is worse than the effectivity of η . Finally, we run the same experiment but for different diffusion coefficients $\varepsilon = 10^{-4}, 10^{-6}, 10^{-8}$ and display in Figure 9(b) the effectivity index of η . We note that it always remains below 4.

5.4 Convection dominated problem

In this section we perform the same experiment as in Section 5.3 but instead of choosing $\beta = (0, 0)^\top$ we set $\beta = -(1, 1)^\top$, hence we solve a nonsymmetric singularly perturbed problem. The linear systems are solved with the GMRES method preconditioned with the incomplete LU factorization.

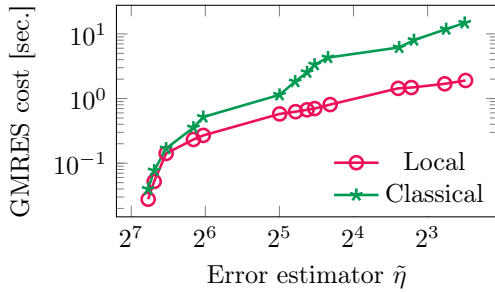


(a) Effectivity index of $\hat{\eta}$.

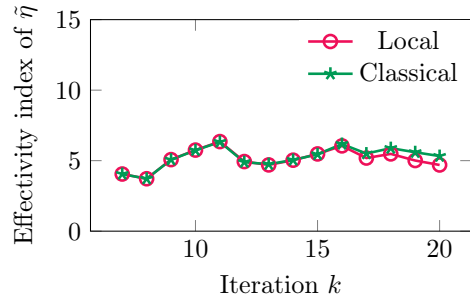


(b) Effectivity index of η for different diffusion coefficients ϵ .

Figure 9. Section 5.3, reaction dominated problem. Effectivity index of $\hat{\eta}$ and of η but for different diffusion coefficients ϵ .



(a) GMRES cost versus $\hat{\eta}$.



(b) Effectivity index of $\hat{\eta}$.

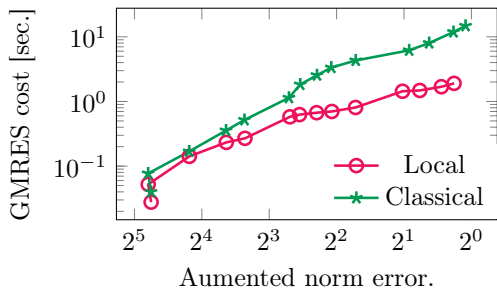
Figure 10. Section 5.4, convection dominated problem. Computational cost vs. $\hat{\eta}$ and effectivity index in function of the iteration number.

As in Section 5.3, we investigate the effectivity indexes and efficiency of the local and classical schemes.

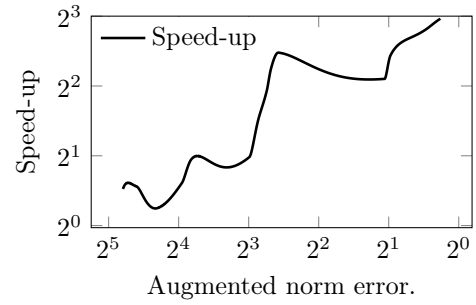
For convection dominated problems, the norm $\|\cdot\|_{\oplus}$ is more appropriate than $\|\cdot\|$ since it measures also the error in the advective direction. In Figure 10(a), we plot the simulation cost versus the error estimator $\hat{\eta}$, we remark that again the local scheme provides similar error bounds at smaller cost. The effectivity index of $\hat{\eta}$ is displayed in Figure 10(b), we note that the local and classical schemes have again similar effectivity indexes.

In Figure 11 we plot the simulation cost versus the error in the augmented norm $\|\cdot\|_{\oplus}$ and the relative speed-up. We again observe that the local scheme is faster.

For completeness, we plot in Figure 12(a) the effectivity index of η . We see that it is completely off. This illustrates that this estimator does not capture the convective error and is hence not appropriate for convection dominated problems. Then, we run again the same experiment but considering different diffusion coefficients $\epsilon = 10^{-4}, 10^{-6}, 10^{-8}$ and display the effectivity indexes of $\hat{\eta}$ in Figure 12(b).

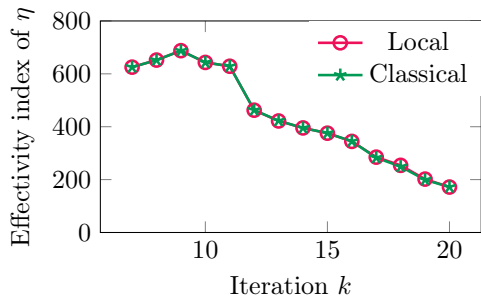


(a) GMRES cost versus augmented norm error.

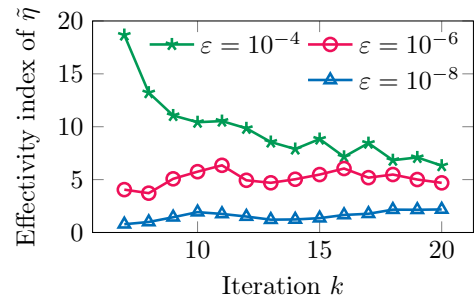


(b) Speed-up in function of the error.

Figure 11. Section 5.4, convection dominated problem. Computational cost vs. augmented norm error and speed-up in function of the error.

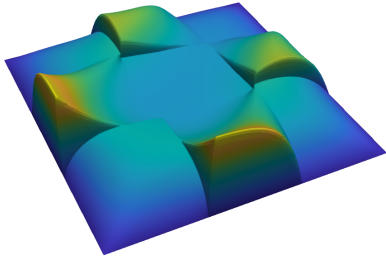


(a) Effectivity index of η .

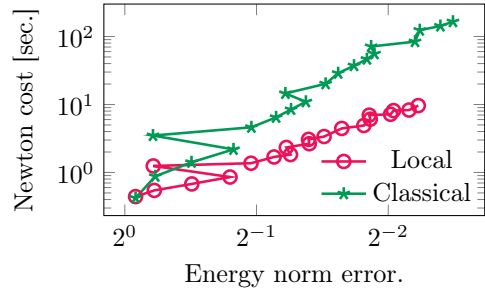


(b) Effectivity index of $\tilde{\eta}$ for different diffusion coefficients ε .

Figure 12. Section 5.4, convection dominated problem. Effectivity index of η and of $\tilde{\eta}$ but for different diffusion coefficients ε .



(a) Solution $u(\mathbf{x})$ of the nonlinear nonsmooth problem.



(b) Newton cost versus energy norm error.

Figure 13. Solution $u(\mathbf{x})$ and efficiency experiment on the nonlinear nonsmooth problem of Section 5.5.

5.5 A nonlinear nonsmooth problem with multiple local structures

We conclude with an experiment on a nonlinear nonsmooth problem, where the diffusion tensor is solution dependent and has multiple discontinuities, hence the solution presents several local structures. More precisely, we solve (1.1) with $\Omega = [-3/2, 3/2] \times [-3/2, 3/2]$, $\beta = -(1, 1)^\top$, $\mu = 1$ and $f(\mathbf{x}) = \|\mathbf{x}\|^2$. The diffusion tensor is $A(u, \mathbf{x}) = A_1(u)A_2(\mathbf{x})$, with $A_1(u) = 1/\sqrt{1+u^2}$. We divide Ω in nine squares of size $1/2 \times 1/2$ and $A_2(\mathbf{x})$ alternates between 1 and 0.01, in a checkerboard-like manner. A reference solution is displayed in Figure 13(a).

Theorems 3.1 and 3.2 do not apply straightforwardly as the problem is nonlinear. Nevertheless, Algorithm 1 can be used in combination with a Newton scheme as it is shown in [1]. In this experiment we investigate the efficiency of the error estimators in identifying the local subdomains for a nonlinear nonsmooth problem with multiple local structures. Starting with a 32×32 elements mesh, we run the code and let it automatically select the subdomains for twenty iterations. We do the same with the classical Algorithm 2 and compare the results in Figure 13(b), where we display the cost of the Newton method versus the error, computed in energy norm, against a reference solution. We remark as the local method is faster.

6 Conclusion

In this paper we have derived a local adaptive discontinuous Galerkin method for the scheme introduced in [1]. The scheme, defined in Section 2.2, relies on a coarse solution which is successively improved by solving a sequence of localized elliptic problems in confined subdomains, where the mesh is refined. Starting from error estimators for the symmetric weighted interior penalty Galerkin scheme based on conforming potential and fluxes reconstructions, allowing for flux jumps across the subdomains boundaries we have derived new estimators for the local method and proved their reliability in Theorems 3.1 and 3.2. An important property of the original estimators (for nonlocal schemes) is conserved: the absence of unknown constants. Numerical experiments confirm the error estimators' effectivity for singularly perturbed convection-reaction dominated problems and illustrate the efficiency of the local scheme when compared to a classical adaptive algorithm, where at each iteration the solution on the whole computational domain must be recomputed. We also showed that the growth of boundary error indicators (the reason why efficiency cannot be proved in general) can be monitored in order to switch from local to a nonlocal method. Switching automatically from local to classical scheme, based on the indicators $\eta_{\Gamma,1}$, $\eta_{\Gamma,2}$, could be easily integrated in a finite

element code. Testing such an integrated code could be of interest to investigate in the future.

Acknowledgments

The authors are partially supported by the Swiss National Science Foundation, under grant No. 200020_172710.

References

- [1] A. Abdulle and G. Rosilho de Souza. A local discontinuous Galerkin gradient discretization method for linear and quasilinear elliptic equations. *ESAIM: Mathematical Modelling and Numerical Analysis*, 53(4):1269–1303, 2019.
- [2] M. Ainsworth. A synthesis of a posteriori error estimation techniques for conforming, non-conforming and discontinuous Galerkin finite element methods. In *Recent advances in adaptive computation*, volume 383 of *Contemporary Mathematics*, pages 1–14. Amer. Math. Soc., Providence, RI, 2005.
- [3] M. Ainsworth and J. T. Oden. A unified approach to a posteriori error estimation using element residual methods. *Numerische Mathematik*, 65(1):23–50, 1993.
- [4] D. N. Arnold. An interior penalty finite element method with discontinuous elements. *SIAM Journal on Numerical Analysis*, 19(4):742–760, 1982.
- [5] I. Babuška and W. C. Rheinboldt. A-posteriori error estimates for the finite element method. *International Journal for Numerical Methods in Engineering*, 12(10):1597–1615, 1978.
- [6] I. Babuška and W. C. Rheinboldt. Error estimates for adaptive finite element computations. *SIAM Journal on Numerical Analysis*, 15(4):736–754, 1978.
- [7] R. E. Bank and A. Weiser. Some a posteriori error estimators for elliptic partial differential equations. *Mathematics of Computation*, 44(170):283–301, 1985.
- [8] L. Barbié, I. Ramière, and F. Lebon. An automatic multilevel refinement technique based on nested local meshes for nonlinear mechanics. *Computers and Structures*, 147:14–25, 2015.
- [9] A. Brandt. Multi-level adaptive solutions to boundary-value problems. *Mathematics of Computation*, 31(138):333–390, 1977.
- [10] F. Brezzi and M. Fortin. *Mixed and hybrid finite element methods*, volume 15 of *Springer Series in Computational Mathematics*. Springer-Verlag, New York, 1991.
- [11] I. Cheddadi, R. Fučík, M. I. Prieto, and M. Vohralík. Guaranteed and robust a posteriori error estimates for singularly perturbed reaction-diffusion problems. *ESAIM: Mathematical Modelling and Numerical Analysis*, 43(5):867–888, 2009.
- [12] S. Cochez-Dhondt and S. Nicaise. Equilibrated error estimators for discontinuous Galerkin methods. *Numerical Methods for Partial Differential Equations*, 24(5):1236–1252, 2008.
- [13] D. A. Di Pietro and A. Ern. *Mathematical aspects of discontinuous Galerkin methods*, volume 69 of *Mathématiques et Applications*. Springer, Berlin and Heidelberg, 2012.

- [14] W. Dörfler. A convergent adaptive algorithm for Poisson’s equation. *SIAM Journal on Numerical Analysis*, 33(3):1106–1124, 1996.
- [15] A. Ern, S. Nicaise, and M. Vohralík. An accurate H(div) flux reconstruction for discontinuous Galerkin approximations of elliptic problems. *Comptes Rendus Mathématique*, 345(12):709–712, 2007.
- [16] A. Ern and A. F. Stephansen. A posteriori energy-norm error estimates for advection-diffusion equations approximated by weighted interior penalty methods. *Journal of Computational Mathematics*, 26(4):488–510, 2008.
- [17] A. Ern, A. F. Stephansen, and M. Vohralík. Guaranteed and robust discontinuous Galerkin a posteriori error estimates for convection-diffusion-reaction problems. *Journal of Computational and Applied Mathematics*, 234(1):114–130, 2010.
- [18] A. Ern, A. F. Stephansen, and P. Zunino. A discontinuous Galerkin method with weighted averages for advection-diffusion equations with locally small and anisotropic diffusivity. *IMA Journal of Numerical Analysis*, 29(2):235–256, 2009.
- [19] W. Hackbusch. Local defect correction method and domain decomposition techniques. In K. Böhmer and H. Stetter, editors, *Defect Correction Methods*, Computing Supplementa, pages 89–113. Springer, Wien, 1984.
- [20] O. A. Karakashian and F. Pascal. A posteriori error estimates for a discontinuous Galerkin approximation of second-order elliptic problems. *SIAM Journal on Numerical Analysis*, 41(6):2374–2399, 2003.
- [21] K. Y. Kim. A posteriori error estimators for locally conservative methods of nonlinear elliptic problems. *Applied Numerical Mathematics*, 57(9):1065–1080, 2007.
- [22] B. S. Kirk, J. W. Peterson, R. H. Stogner, and G. F. Carey. libMesh : a C++ library for parallel adaptive mesh refinement/coarsening simulations. *Engineering with Computers*, 22(3-4):237–254, 2006.
- [23] S. McCormick and J. Thomas. The Fast Adaptive Composite grid (FAC) method for elliptic equations. *Mathematics of Computation*, 46(174):439–456, 1986.
- [24] J. Nédélec. Mixed finite elements in \mathbb{R}^3 . *Numerische Mathematik*, 35(3):315–341, 1980.
- [25] L. Payne and H. Weinberger. An optimal Poincaré inequality for convex domains. *Archive for Rational Mechanics and Analysis*, 5(1):286–292, 1960.
- [26] P. Raviart and J. Thomas. A mixed finite element method for 2nd order elliptic problems. In E. Magenes and I. Galligani, editors, *Mathematical aspects of finite element methods (Proc. Conf., Consiglio Naz. delle Ricerche (C.N.R.), Rome, 1975)*, volume 606 of *Lecture Notes in Mathematics*, pages 292–315, New York, 1977. Springer-Verlag.
- [27] G. Rosilho De Souza. *Numerical methods for deterministic and stochastic differential equations with multiple scales and high contrasts*. PhD thesis, EPFL, Lausanne, 2020.
- [28] A. F. Stephansen. *Méthodes de Galerkin discontinues et analyse d’erreur a posteriori pour les problèmes de diffusion hétérogène*. PhD thesis, Ecole Nationale des Ponts et Chaussées, 2007.

- [29] R. Verfürth. *A review of a posteriori error estimation and adaptive mesh-refinement techniques*. Wiley-Teubner, New York, 1996.
- [30] M. Vohralík. Residual flux-based a posteriori error estimates for finite volume and related locally conservative methods. *Numerische Mathematik*, 111(1):121–158, 2008.